METEOROID STREAM SOURCES FROM DYNAMIC AND PROBABILISTIC TRAJECTORY ANALYSIS

By

LARS GÖRAN ADOLFSSON

A DISSERTATION PRESENTED TO THE GRADUATE SCHOOL
OF THE UNIVERSITY OF FLORIDA IN PARTIAL FULFILLMENT
OF THE REQUIREMENTS FOR THE DEGREE OF
DOCTOR OF PHILOSOPHY

UNIVERSITY OF FLORIDA

1996

To Madeleine, Christopher and Danniella

ACKNOWLEDGMENTS

It is a pleasure to thank the members of my examining committee, Humberto Campins, Stanley Dermott, Bo Gustafson, Carl Murray, and Yngve Öhrn. I owe special thanks to Bo Gustafson for serving as chairman on my committee.

Bo has shown me that there is another side to science than just being able to "put up" equations. He always want to think physically about the problem at hand, something I wish to master one day. I also value very much the many long talks we have had on how to survive in science. I firmly belive that it should be part of the curriculum. Lastly I wish to thank Bo for his friendship!

During my first couple of days in graduate school, far from home, I realized how different this country was from my own. Keith Grogan, the "Liverpuddlian", helped me stay (almost) sane throughout graduate school. I wish to thank Keith for conversations, beers, soccer-updates, taking care of first submissions, and many more things. I thank all faculty and graduate students for very interesting years. Special thanks goes to Seppo Laine, Sumita Jayaraman, Dave Osip, Tim Spahr, Joanna Thomas-Osip, and Steve Kortenkamp.

I wish to express deep gratitude to my parents, Karin and Hugo Adolfsson, for their support and almost endless interest in my work.

Finally, I thank Madeleine for all the love and emotional support she has given me through many difficult times, and all the happiness she has shared with me through good times.

TABLE OF CONTENTS

ACKNOWLEDGMENTS iii

ABSTRACT vi

CHAPTER 1: INTRODUCTION 1

Meteoroids and Streams 1
Identification of Meteoroid Stream Sources 4

CHAPTER 2: PRODUCTION OF METEOROIDS 8

Cometary Activity 10
Collisions 16

CHAPTER 3: METEOROID DYNAMICS 19

Cometary Coma 19
Collisions 23
Interplanetary Space 24
Atmospheric Flight 31

CHAPTER 4: PARENT-DAUGHTER ASSOCIATION METHOD 36

Sampling of Error Distributions and Orbital Integrations 38
Meteoroids 39
Parent Bodies 44
Intersection Condition 45
Ejection Condition 47
Probability Computations 48

CHAPTER 5: OBSERVATIONAL MATERIAL AND DATA REDUCTION 52

Meteoroids 52
Harvard Small Camera Program 54
Harvard Super-Schmidt Program 60
Prairie Network 66
Parent Bodies 73

Geminids: 3200 Phaethon, 1566 Icarus, 5786 Talos 73
Taurids: P/Encke 74
Computations and Hardware 75

CHAPTER 6: CROSS-SECTION TO MASS RATIO 77

CHAPTER 7: RESULTS 82

Geminids 82
Taurids 92

CHAPTER 8: DISCUSSION 96

CHAPTER 9: CONCLUSIONS 112

REFERENCES 114

BIOGRAPHICAL SKETCH 120

Abstract of Dissertation Presented to the Graduate School
of the University of Florida in Partial Fulfillment of the
Requirements for the Degree of Doctor of Philosophy

METEOROID STREAM SOURCES FROM DYNAMIC AND PROBABILISTIC TRAJECTORY ANALYSIS

By

Lars Göran Adolfsson

May 1996

Chairperson: Bo Å. S. Gustafson
Major Department: Astronomy

We develop a method to estimate the probability of a genetic relation between a specific meteoroid and a proposed parent body. From meteor data, using single-body meteor theory, we estimate the errors in the velocity vector and the cross-section to mass ratio of the meteoroid. We sample these errors and probe the orbit probability distribution by numerically integrating the equations of motion back in time. The integrations account for planetary perturbations, radiation pressure, Poynting-Robertson light drag, and solar wind corpuscular drag.

Two conditions are used to ensure the opportunity of a genetic relation. First, we require that the orbits of the meteoroid and the parent body intersect; the intersection condition. Identification of an ejection point allows estimates of ejection conditions; relative velocity, direction of ejection, heliocentric distance, and epoch of ejection. Secondly, an intersection point is rejected as a potential ejection site unless the relative velocity is deemed

to be a physically realistic ejection velocity; the ejection condition. The probability of a genetic relation is estimated as the fraction of the sampled orbits that satisfy both criteria.

The method is applied to Geminid and Taurid meteors. Only the most precise meteors are considered. A total of 55 Geminids from the Harvard Small Camera Program, the Harvard Super-Schmidt Program, and the Prairie Network, are used. Twenty-six Taurids from the Harvard Super-Schmidt Program and the Prairie Network are also chosen. The error in velocity is typically 0.01-0.1%. A large error in the velocity vector lead to a situation where we are less likely to find the ejection point and establish a genetic relation.

A genetic relation for 28 of the Geminids and their proposed parent body Phaethon is established, indicating cometary activity as the formation process. Phaethon was probably active over at least 5,000 years, terminating its activity as recently as $\approx$ AD 1,800. None of the Taurids satisfy all criteria within the method, and could not be linked to their proposed parent body comet P/Encke.

CHAPTER 1
INTRODUCTION

Meteoroids and Streams

Meteoroids are small interplanetary bodies orbiting the Sun. Meteoroids come in a wide range of sizes; considerably larger than atoms and up to a size comparable to the smallest asteroids. However, no hard-and-fast boundaries exist. A size range below 100 μm is usually implied by the word dust, a subset of meteoroids.

The word meteor is a general term describing the luminous track and the ionization associated with the entry of a meteoroid into the atmosphere (see Bronshten, 1983, for a thorough review of meteor phenomena). The apparent maximum brightness of a meteor is, to first approximation, proportional to the mass of the meteoroid. Since the mass (proportional to the size to the third power) range of meteoroids is wide, this implies that the same holds true for the range of the maximum brightness of meteors.

The faintest meteors (not observable to the naked eye) are observed through the use of radar, and they are subsequently described as radar meteors. Most people have at some time or other seen a "shooting star" or a "falling star." This corresponds to a visual or photographic meteor. The brightest, and most rare, meteors, brighter than Venus and occasionally rivaling the Moon, are denoted fireballs.

The meteoroid material that survives atmospheric entry, and reaches the surface of the Earth, is called a meteorite. It has to be noted, though, that every meteoroid impacting the Earth's atmosphere does not produce a meteorite. A meteoroid made of a tough material and impacting the atmosphere at low speed, is much more likely to produce a meteorite, than a meteoroid made of a friable material which is prone to fragment, and impacting the atmosphere at high speed.

While it holds true that a large enough meteoroid will produce a meteorite, it is also true for a small enough meteoroid (although it is usually close to or within the size range of dust). The kinetic energy (proportional to the square of the impact speed) of the meteoroid is, to first approximation, converted into heating, sublimation, and thermal radiation of the meteoroid. The sublimation is extremely dependent on the surface temperature. A small meteoroid, with a large cross-section to mass ratio, can effectively control the temperature through thermal radiation, and at the same time it is decelerating at a high rate (Whipple, 1950a). This has the implication that the meteoroid can escape sublimation and slowly sediment through the atmosphere. These meteoroids, called micro-meteoroids or micro-meteorites, may then be collected in the Earth's stratosphere (Brownlee, 1978), and are then called interplanetary dust particles (IDPs).

On certain calendar dates, the number of observed meteors is greater than the average. In addition, it is found that the meteor trails, when projected back, are emanating from a common point on the celestial sphere -- the radiant. This is an effect of perspective; the meteoroids all enter the atmosphere along roughly parallel tracks. These attributes constitute the annual meteor showers.

In general, a meteoroid stream is a large number of meteoroids travelling around the Sun in similar orbits. If it is such that the meteoroid stream intersects the orbit of the Earth, it

will produce an annual meteor shower. This implies that on the Earth, we are only able to observe a tiny fraction of the meteoroid streams in our Solar System.

A meteoroid stream is not a static phenomenon. Due to planetary perturbations and differences in forces acting on meteoroids of different sizes, the orbits of the individual meteoroids will become less similar. Eventually it is not possible to distinguish the meteoroid stream from the sporadic background. From this it is also seen that the annual meteor showers observed at the present epoch were not observed in the past, and they will not be observed at some future time.

The annual meteor showers usually show the same level of activity, with minor fluctuations, year after year; implying that the meteoroids are equally distributed along the stream orbit. However, an intense outburst of activity, significantly above the regular value, is sometimes observed (cf. Jenniskens, 1995). This is called a meteor outburst or meteor storm, and is usually associated with the recent ejecta of comets such that the meteoroids have not yet spread out along the orbit. The most famous meteor storm is that of the Leonids.

There are several conceivable sources for meteoroids. For example, the decay of comets through cometary activity, collisions among asteroids and the subsequent collisions between fragments, impact ejecta from planetary or satellite surfaces, production through volcanism (Jupiter's moon Io), and interstellar origin.

This thesis will develop the first method to rigorously and quantitatively identify the source of a specific meteoroid. Although the method may readily be applied to a sporadic meteoroid, it is better to derive some of the conditions at ejection. We may also apply it to meteoroid streams with already proposed parent bodies. It is then possible to test the method against less elaborate techniques of identifying meteoroid sources, and judge their merits.

Identification of Meteoroid Stream Sources

Without referring to any particular meteoroid stream or comet, Daniel Kirkwood (1861) may have been the first to suggest a connection between the two phenomena. Giovanni Schiaparelli (1867) found that the periodic comet P/Swift-Tuttle gave the correct radiant for the annual Perseid meteor stream, corroborating Kirkwood's suggestion. So far, all meteor observations had been made by the naked eye, and to establish more rigorous connections between meteoroid streams and comets, it became apparent that the quality of the observations must improve.

Although the method of photographing a meteor - to determine its trajectory, velocity, and deceleration - is simple and effective, no important results were reached until the advent of the double station program at the Harvard Observatory (Whipple, 1938). Two cameras, with a baseline of 38 km, were directed towards a point in space about eighty kilometers above the Earth's surface. Unfortunately, the cameras were not originally designed for meteor photography; only about five meteors were simultaneously photographed per year. The Harvard Meteor Program (Jacchia & Whipple, 1956) increased the observation rate by a factor of $\approx$ 1,000. This program utilized Baker Super-Schmidt cameras, custom designed for meteor photography.

Whipple and Hamid (1952) used nine doubly photographed Taurid meteors from the Harvard Meteor Program to establish a connection between the annual Taurid meteor shower and comet P/Encke. Using analytical expressions for the secular perturbations by Jupiter, the authors tentatively proposed that the Taurid streams (the Northern and Southern branch) were formed by a violent ejection, as a result of encounters with small asteroidal bodies, of material from P/Encke some 4,700 and 1,400 years ago.

As the reduction (made by hand, c.f., Whipple & Jacchia, 1957) of many Harvard Meteor Program photographs became complete, it was possible to use statistical methods on the orbital data. Southworth and Hawkins (1963) developed a quantitative criterion, the D-criterion, for stream membership based on a measure of orbit similarity. The obvious advantage of such a criterion is that an old, dispersed or tenuous stream might be identified on statistical grounds, and distinguished from the sporadic background. However, the value of the criterion had to be determined empirically, based on values found for previously known major streams. Further, the criterion only measures the orbits similarity at the epoch of the meteors, not the epoch of ejections. The orbital evolution, due to planetary perturbations and non-gravitational forces, is not accounted for. Drummond (1981) made slight modifications to the D-criterion, which he then called the D'-criterion, but it is still plagued by the same shortcomings previously mentioned.

Sekanina (1970) refined the criterion for stream membership. Instead of having one limit of the D-criterion, Sekanina used different values of the criterion for different meteoroid streams. This is justified due to the fact that streams disperse into the sporadic background on different time scales, due to differences in the dynamical behavior of the heliocentric trajectories. However, Sekanina's method does not account for the dynamical evolution of a specific meteoroid trajectory, only for the stream as a whole.

A leap in the understanding of meteoroid streams was made possible through computers and effective numerical algorithms. The use of a computer allows fast integration of the equations of motion for a large number of meteoroids, both forward and backward in time (since the equations of motion are time-reversible).

Forward integrations can be used to forecast the activity of a meteor shower (e.g., Fox et al., 1983). A timely example of this is the estimate of the Leonid meteor storm, expected to

occur in November 1998 or 1999 (Brown & Jones, 1993). Such simulations requires estimates of several unknown parameters associated with the meteoroid stream formation; the epoch, the heliocentric distance, and the velocity (direction and magnitude) at ejection, the size of the meteoroid, and the non-gravitational forces acting in interplanetary space. It may be argued that the forward integration of several thousands of ejected, hypothetical meteoroids from an assumed epoch and conditions of ejection would accurately describe the present or future extent of the meteoroid stream. However, since it is not certain that the estimates of the parameters mentioned above are close to the real values, forward integrations have to be treated cautiously.

Backward integrations are used to find a genetic relation between a meteoroid stream and a proposed parent body (Kramer & Shestaka, 1986; Gustafson, 1989b, Froschlé et al., 1993). Gustafson (1989b) used the orbits of twenty doubly photographed (Harvard Meteor Program) Geminids, and traced them to cometary activity on 3200 Phaethon (it was classified as an Apollo asteroid, and subsequently given the number 3200) within the last 2,000 years. The author thereby eliminated the need for estimates of the parameters mentioned in the previous paragraph.

This thesis is a refined version of Gustafson's (1989b) work. It is an extension in two important ways. First, the atmospheric entry process of a meteoroid has been evaluated, and the pre-atmospheric cross-section to mass ratio of the meteoroid is estimated (Gustafson & Adolfsson, 1996). Secondly, the integrations backward in time start from the top of the atmosphere, where all input parameters - the pre-atmospheric velocity (direction and magnitude) and cross-section to mass ratio - are estimated with corresponding uncertainties. This allows a probabilistic treatment; a number of meteoroid trajectories are sampled from the uncertainty distribution and integrated back in time, where conditions for ejection from a

proposed parent body can be evaluated. It is then possible to estimate the probability that a specific meteoroid was produced by a specific parent body. This is the first time that a meteoroid is rigorously connected to its source. It should also be pointed out that the thesis method directly provides estimates for the parameters needed as input to forward integrations.

Chapter 2 is devoted to a general description of the two mechanisms of meteoroid production considered in this thesis; cometary activity and collisions. Chapter 3 describes the meteoroid dynamics from the "birth" (cometary activity or collision), through its "life" in interplanetary space, all the way to its "death" at atmospheric entry. The theory of the method, to relate a specific meteoroid to its proposed parent body, is explained in chapter 4. The observational material and the data reduction is presented in chapter 5. The interpretation of the estimated meteoroid cross-section to mass ratios is discussed in chapter 6. Chapter 7 gives the results obtained when the method is applied to observations, and is followed by a discussion (Chapter 8) and conclusions (chapter 9).

CHAPTER 2
PRODUCTION OF METEOROIDS

Meteoroids are distributed throughout the Solar System. Complementary to ground-based are in-situ observations by dust impact detectors on board interplanetary space probes. In-situ measurements of interplanetary meteoroids have been performed in the heliocentric distance range from 0.3 AU out to 18 AU. To model the interplanetary meteoroid data (ranging from 10^{-18} to 1 g in mass and 0.1 to 20 AU in heliocentric distance), Divine (1993) required five distinct populations described by particle mass, perihelion distance, eccentricity, and inclination. The important question if these different populations are truly different in origin, or if they are merely a convenient description, still awaits its answer.

A second important question is if the meteoroid complex is in equilibrium. The sink for the meteoroid complex is in the small meteoroid range (dust), where the Poynting-Robertson light drag (cf. chapter 3) dissipates orbital angular momentum, causing the meteoroid to slowly spiral towards the Sun. An additional effect, feeding more material into the small meteoroid range, is collisions among meteoroids (Grün et al., 1985). The sources for meteoroids are usually thought to be comets or asteroids. The question as to whether the supply of meteoroids through these sources adds up to the material lost is still unanswered, although it is most probable that the complex is in non-equilibrium (Grün et al., 1985).

The primary source of meteoroids in the zodiacal cloud is either asteroidal or cometary. Zodiacal light can be observed from low light pollution areas on the Earth with the unaided eye. It appears as a diffuse glow in the west after sunset and in the east before dawn.

For centuries it has been accepted wisdom that zodiacal light is caused by reflection of sunlight from a large number of small meteoroids which are concentrated in the ecliptic plane. The Infrared Astronomical Satellite (IRAS) detected zodiacal dust bands, which led to the identification of distinct asteroid families as their source (Dermott et al., 1984). However, asteroids are not the only source. Direct evidence of the input of comets to the zodiacal cloud was found by Sykes and Walker (1992) in the cometary dust trail observed (again) by IRAS. The fraction of asteroidal to cometary material in the zodiacal cloud is estimated as one-third (Dermott et al., 1994). It has to be noted, though, that the modeling of the zodiacal cloud, and its comparison with observations, is complex, requiring attention of the dynamics as well as the optical and thermal properties of the meteoroids (Gustafson, 1994).

The Ulysses spaceprobe has provided evidence for two additional sources of meteoroids; the jovian system and interstellar space. Ulysses detected small meteoroids (mass $\leq 2.5\times10^{-14}$ g), within a few months of Jupiter fly-by in early 1992, in collimated streams with a remarkable periodicity of 28±3 days, and with the streams radiating from close to the line-of-sight direction to Jupiter. Several mechanisms have been suggested, but it is clear that the streams originate from within the jovian system (Zook et al., 1996). While the meteoroids emitted from the jovian system are characterized by their smaller masses and their narrow bunching both in time and impact direction, there appears to be an interstellar origin for other meteoroids (Grün et al., 1993). The evidence came from consideration of the impact direction and speed of the meteoroids. They are distinguished from interplanetary meteoroids since they are on retrograde trajectories, with a speed above the maximum speed possible for a bound heliocentric orbit.

There are even more suggested sources of meteoroids, including ejecta from planetary and satellite surfaces. This is based on the evidence that some meteorites found on Earth

appear to be of lunar or Martian origin. These meteorites, however, are much larger than the meteoroids found during in-situ measurements. Before we discuss the production of meteoroids from the two main sources - comets and asteroids - it is interesting to compare meteoroids to other bodies in the Solar System.

A "back of the envelope" calculation of the mass of the present meteoroid complex, accounting only for the short-period cometary component, yields an estimate of $\approx 3 \times 10^{20}$ g (Hughes, 1993). This is of comparable mass to a small asteroid or a small moon, e.g., Pluto's moon Charon. With this in mind, i.e., the negligible mass of the meteoroid complex with respect to other Solar System bodies, it is truly remarkable how much information meteoroids provide. However, while the mass of the other Solar System bodies is much larger (by a factor $\approx 10^{10}$, excluding the Sun), they are truly outnumbered by the meteoroids. We may view meteoroids as probes, by which we may reveal some aspects of the origin and evolution of the Solar System.

Cometary Activity

Comets have been observed since the dawn of mankind. The appearance of a bright comet has always been of great interest, but only in recent years has it become possible to explain in some detail the physical causes of such spectacular displays (e.g., Huebner, 1990).

It is customary to define four major constituents of a comet. First, there is the cometary nucleus, a kilometer-sized, irregularly shaped, solid body of relatively loose internal cohesion, consisting of ices (mostly water-ice) with imbedded dust particles. Second is the coma, a gaseous dusty atmosphere around the nucleus, which develops as the comet approaches the Sun, and becomes less pronounced on the comets motion away from the Sun. The coma consists of evaporated molecules and their daughter products (radicals, atoms, ions)

as well as meteoroids released in the same process. Depending on the "active" areas (found to be 10-20% of the total surface area on P/Halley) on the surface on the nucleus, the coma may be featureless or highly structured. Third is the dust tail, consisting of small meteoroids that are lost from the coma and subject to solar radiation pressure (chapter 3). Last is the ion tail consisting of ions lost from the coma, and accelerated in the anti-solar direction by the interplanetary magnetic field, carried by the solar wind.

A major revolution in cometary science took place in 1950-1951, when three fundamental ideas were formulated. (1) Fred L. Whipple (1950b; 1951) proposed his icy conglomerate, solid nucleus model. Whipple's model had the virtue of explaining several cometary features; the large gas production rates, the observed jet-like structures in the coma, the observed non-gravitational orbital motion, the survival of some Sun-grazing comets with perihelion distances of less than 0.005 AU, and that comets are the source of meteoroid streams. (2) Jan H. Oort (1950) deduced the existence of a cometary reservoir, the Oort cloud, by studying the distribution of the semi-major axes of 19 observed comets. Oort estimated that the cloud must contain about 2×10^{11} comets, with a mean distance of 50,000 AU. With an average mass of 10^{16} g, the total mass of the Oort cloud would be roughly one-third of the Earth's mass. Present estimates yield 10^{12} comets of a mass a few times that of the Earth. (3) Ludwig Biermann (1951) explained the motion of the cometary plasma as due to interaction with the solar wind.

Another revolution in cometary science took place in March 1986 as six spacecraft observed P/Halley in-situ. The enormous amount of data acquired during this encounter, and the subsequent (but not exhaustive) analysis thereof, has already made present cometary scientist talk of the "pre- and post-Halley" eras. The findings on cometary meteoroids from this campaign will be discussed later in this section.

Comets are usually divided into two categories, depending on their orbital periods; long-period (period > 200 years), and short-period (period < 200 years, and denoted with "P/," e.g., P/Halley with period 76 years). One further distinction is also customary; those comets with an orbital period < 20 years are denoted Jupiter family comets, since their orbital evolution is controlled by Jupiter, and those short-period comets with an orbital period > 20 years are denoted Halley-type comets (after the prototype P/Halley). According to the catalogue by Marsden and Williams (1993), we have observed 681 long-period comets (observed only at one apparition) and 174 short-period comets.

The standard scenario for the origin of cometary nuclei is the agglomeration of interstellar grains in the presolar cloud or the solar nebula. The capture of comets from interstellar space, implying that they are not original members of the Solar System, appears to be less probable due to, e.g., low capture efficiency (Valtonen & Innanen, 1982). The formation of comets, as icy planetesimals in the Uranus-Neptune accretion zone, gives evidence for the Oort cloud. Comets would thus have been gravitationally scattered, partly into long-period orbits, by proto-Uranus and proto-Neptune. Numerical simulations (Duncan et al., 1987) show that after 4.5×10^9 years (the estimated age of the Solar System), most comets (80-90%) are situated in an inner core (inside 20,000 AU) and the rest in the outer parts; the classical Oort cloud.

An additional formation site is beyond Neptune's orbit. The idea was first championed by G. Kuiper (1951), who did not like the apparent emptiness of the outer solar system. The region was denoted the Kuiper belt, and its existence is supported through recent discoveries of trans-Neptunian objects (see, e.g., Luu, 1994). Long-period comets are thought to originate in the Oort cloud; comets are injected into the inner Solar System by perturbations due to passing stars, tides from the galactic disk, or massive molecular clouds. However, the idea that

the Oort cloud also supplies the short-period comets, has come under attack. Duncan et al. (1988) demonstrated that a better alternative source may be found in a comet belt, outside the outer planets, the Kuiper belt.

An important question arises as we address the nature of the meteoroids produced through cometary activity. Out of what material, and to what degree has it been processed, were comets formed, 4.5×10^9 years ago? A model which has met with considerable success, and is generally viewed as a useful concept, is the "Bird's-Nest" model, originally proposed by Greenberg and Gustafson (1981). The "Bird's-Nest" model represents the dust as pieces of bulk cometary material of aggregated nebular dust, from which the volatile ices (mainly water) have sublimated. During the 4.5×10^9 years that the comet nucleus is part of the Oort cloud or the Kuiper belt, the ices in its surface layer have been altered by ultraviolet radiation and cosmic rays. The interior may have undergone similar changes from residual nuclear activity, from conversion of kinetic energy into energy of deformation, and heat during the collisions in the aggregation process.

As a cometary nucleus enters the inner Solar System, its lifetime as a reasonably bright comet is only a small fraction of the age of the Solar System. An additional effect, apart from the limited budget of material, that may choke cometary activity is the development of a dust mantle (e.g., Rickman et al., 1990). From the Giotto images of the P/Halley nucleus, it was discovered that distinct dust jets, emanating from a sunlit side and fed by local outgassing, were restricted to a few "active regions" (10-20% of the nucleus surface). It is quite probable that the inactive surface areas of P/Halley is due to a dust mantle. Eventually, the surface of the nucleus may be completely covered by a dust mantle, and the cometary activity ceases. The identification of asteroid 1979 VA with comet P/Wilson-Harrington implies that the comet transformed into a dormant state. Another example is the proposed parent body of the Geminid

meteoroid stream, asteroid 3200 Phaethon, which today shows no sign of cometary activity, and may be extinct (no volatiles left) or dormant.

Some models find that a dust mantle thickness of no more than a few centimeters is enough to quench the gas flow nearly completely. As a result, its thickness increases slowly, and it may be subject to disruption either by an impacting meteoroid or by the underlying gas pressure exceeding its weight and cohesion. Therefore it is likely that "blow-offs" may occur as a general feature of dust mantle models. Based on these physical arguments, Gustafson (1992) argued that cometary meteoroids may be shaped as flakes, rather than according to the customary spherical assumption, implying that the meteoroids may attain a higher ejection speed, close to the neutral gas speed (Gustafson, 1989a), as they leave the coma.

Upon sublimation of the ices, the cometary meteoroids are entrained in the gas stream, leaving the nucleus. The meteoroids are decoupled from the gas, attaining their terminal velocity, at a distance of about a few hundred km, and are then subject to interplanetary forces. Small meteoroids, typically 1 to 10 μm in size, are accelerated by solar radiation pressure into the dust tail, and can be observed from the Earth as they scatter sunlight. Larger meteoroids, of several 100 μm in size (a size which may produce photographic meteoroids), are occasionally, due to geometric effects, observed in a narrow, sunward-directed antitail, opposite to the ordinary dust tail.

Probstein (1969) realized that the large number of molecular collisions in the inner coma allowed a continuum-type gas flow description. Several refinements to this model have been made, but the consensus is that the micrometer-sized or slightly larger meteoroids have a terminal velocity almost reaching the escaping gas (about 1 km sec^{-1}), whereas the centimeter and decimeter-sized meteoroids barely reach the gravitational escape velocity from the nucleus (about 1 m sec^{-1}). However, Crifo (1991) point out that recent indirect determinations of

ejection velocities (Cremonese & Fulle, 1989) conflict with the theoretical estimates; small meteoroids have smaller terminal velocities and large meteoroids have higher terminal velocities, as expected for flakes. To improve our knowledge on the dependence of mass (or size) on the ejection velocities of cometary meteoroids, it is apparent that we require direct, in-situ observations through, e.g., Doppler velocimetry.

Previous to the P/Halley encounters, the meteoroid size distribution was determined solely from optical observations of dust tails (see, e.g., Finson & Probstein, 1968a,b) and from infrared observations (see, e.g., Hanner, 1983). These investigations suggested that the size distribution peaks at a particle size of a few μm. One of the most spectacular events of the P/Halley missions was that the mass-loss rate was governed by the emission of massive meteoroids (see Crifo, 1991, for discussion).

The P/Halley missions allowed, for the first time, collection of comprehensive and direct information on the gas and meteoroid emission (cometary activity) from a comet (see Grün & Jesseberger, 1990, for review). The total gas production rate is about 2×10^7 g sec^{-1}, with an uncertainty of ±50%. The total meteoroid production rate is difficult to model. First, the emission is highly anisotropic, as evidenced by all in-situ meteoroid experiments and camera observations. Further, the uncertainty in the terminal velocities and the fact that most of the massive meteoroids have not been detected, render estimates uncertain. However, considering the chemical composition of the observed meteoroids and the gas, and comparing it with solar abundances, the meteoroid to gas mass ratio can be assigned as 1:1, with an uncertainty of a factor of two. The overall composition of P/Halley is almost of solar abundance.

Another important discovery made from the P/Halley data was the identification of two different types of particles; "CHON" particles (rich in elements H, C, N, and O) and "silicate"

particles (rich in Mg, Si, and Fe). Most observed particles, however, are a variable mixture of these extremes.

The "Bird's-Nest" model predicts porous, fluffy meteoroids. Assuming comet nuclei of bulk densities of 0.6 g cm^{-3} (Rickman, 1989), the mixture of solar nebula material (Greenberg & Hage, 1990) leads to a packing factor (defined as the fraction of volume occupied by material) of ≈ 0.33. In the absence of any compacting process, the depletion of volatiles, leaves behind a "Bird's-Nest", of packing factor ≈ 0.15, a loosely packed tangle of refractory materials (Gustafson, 1994).

It should also be noted that meteoroids released from the nucleus may undergo further processing. If the ejected meteoroids contain volatile ices, they sublimate rapidly. It is then possible that the sublimation will cause stresses in the material, and subsequent fragmentation of the meteoroids.

Collisions

Meteoroids are produced when two objects collide. The outcome of a collision is usually divided into one of two possible outcomes; a catastrophic break-up or a cratering forming event. While collisions can take place throughout the Solar System, the probability of a catastrophic collision between large bodies is highest in the asteroid belt.

The asteroid belt is situated between Mars and Jupiter, within a distance of roughly 2.2 to 3.3 AU. The objects populating this region, on fairly circular orbits in the ecliptic plane, are denoted minor planets or asteroids. The largest asteroid, Ceres, has a diameter and a mass of roughly 1,000 km and 10^{24} g, respectively. The total number of asteroids, which have been observed enough to allow a computation of orbital elements and a numbering of the asteroid,

is around 6,000. The total number of asteroids is much larger, since we can only observe the largest members of the population.

Not all asteroids are situated within the asteroid belt. Trojan asteroids are located in broad regions centered 60° before or 60° after Jupiter, in a 1:1 resonance. Another group, the Apollo asteroids (named after the first observed asteroid in the group), have a larger eccentricty, allowing the asteroid to come closer to the Sun than most other asteroids. Since the Apollo asteroids come closer to the Earth, it is possible to detect many small members of this group. While they are fairly close to the Earth, they are denoted Near Earth Asteroids (NEAs).

It is possible that annual meteoroid streams are produced through collisions with NEAs in the asteroid belt. The NEAs have their aphelion (the furthest distance from the Sun, at which they spend most of their time), somewhere in the inner region of the asteroid belt. A probable scenario is that the NEA collide with a small asteroid (or a large meteoroid, depending on where the limiting size is put), and meteoroids are ejected into orbits similar to that of the NEA parent body.

The velocity distribution of the ejection fragments (meteoroids) are often assumed to follow a power-law distribution with a lower cutoff velocity. This assumption is corroborated by laboratory experiments on hypervelocity impacts (see, e.g., Gault et al., 1963, for cratering; e.g., Nakamura & Fujiwara, 1991, for break-up events).

There is a discrepancy in the efficiency of meteoroid acceleration between collision experiments and the ejection velocities inferred from asteroidal breakup. From the dispersion of orbital elements for the largest members of an asteroid family (asteroids grouped together in terms of their orbital elements and thought to be of common collisional origin), typical ejection velocities of a few 100 m sec^{-1} are easily inferred (Zappalà et al., 1984). On the other

hand, experiments (Gault et al., 1963) indicate ejection velocities ≈ 50 m sec^{-1}. As the reason for this discrepancy is not understood, further experimental and theoretical research is needed (Farinella et al., 1994).

Asteroidal material is different from cometary. While cometary material is thought to be almost pristine, asteroidal material has undergone different processes. Asteroids were formed in the inner part of the solar nebula, where the temperature was too high for ices to exist. Comets, on the other hand, were formed further out in the nebula, where ice did exist, and ices are therefore a major constituent of comets. Further, some asteroids grew in size, and chemical differentiation took place, i.e., the heavier elements, such as iron, sank into the interior of some asteroids.

The asteroids never accreted into a full-size planet. The growth was aborted due to the gravitational influence of the massive Jupiter. Later, after the asteroids formed, they have been subject to collisions (which is seen from their cratered surfaces), producing both asteroid families and numerous smaller fragments, of which a few have been collected as meteorites on Earth.

The connection between meteorites and asteroids is evidenced by the similarity of spectroscopic observations and that the orbits of three meteorites (Pfibram, Lost City, and Innisfree) have their aphelion in the asteroid belt. However, it is important to notice that the Earth's atmosphere is selective; only the "tough" material generate meteorites, and the meteorite sample is therefore biased.

CHAPTER 3
METEOROID DYNAMICS

This chapter presents the essential dynamics of a meteoroid during its life; from its birth (cometary activity or collisions), through its life (interplanetary space), and finally to its death (atmospheric entry).

The meteoroids we consider are those which produce photographic meteors. This implies a characteristic size of the meteoroid larger than ~ 500 μm.

The equations presented are used in the Parent-Daughter association method (chapter 4). Further, the chapter also serves to give upper estimates of the theoretical ejection velocities attained in the ejection process. These expressions are then used in section 4.3, when the condition of ejection is presented.

Throughout the chapter we find that one of the most important parameters is the meteoroid cross-section to mass ratio A/m. How we estimate this parameter from meteor data is discussed in Chapter 5.

Cometary Coma

As the comet approaches the Sun, the ices sublimate, and the meteoroids are entrained in the gas flow. The gas transfers momentum to the meteoroids, which are accelerated. Later, the meteoroids decouple from the tenuous gas, reach their terminal velocity, and are subject to interplanetary forces. While this scenario is simple, there are several complicating processes

involved when we try to estimate the terminal velocity of the meteoroid (see, e.g., review by Gombosi et al., 1986; Huebner, 1990).

The solar radiation reaching the nucleus, supplying energy for sublimation of ices and outflow of meteoroids, must penetrate an extensive, absorbing dusty atmosphere. Any change in the gas and meteoroid production alters the optical characteristics. This causes a "retarded" effect on the production rates of gas and meteoroids.

The radiative transfer problem in the coma is far from simple. The radiation field in the coma can be divided into three parts, the direct solar radiation field, the multiple scattered flux, and the diffuse radiation produced by thermal radiation from the meteoroids. Radiative calculations (Marconi & Mendis, 1984) show that the total radiation flux reaching the nucleus is about 25% higher than the unattenuated solar radiation; consequently, the gas and meteoroid production rates are somewhat larger than they would have been if the optical properties of the coma were neglected.

The P/Halley Giotto images show that the gas and the meteoroids emanate from "jets." To model this phenomenon, a time-dependent, multidimensional treatment, accounting for the irregular shape of the nucleus, is required. A number of investigators (e.g., Gombosi & Horányi, 1986; Crifo et al., 1995) have looked into this phenomenon, and they find that the terminal meteoroid velocities are increased by some 20-30%.

To illustrate the complexity involved when computing the dynamics of a meteoroid, we follow Gombosi et al. (1986). Assume the nucleus to be spherical, of radius R_n, and that the sublimated gas consists of water vapor. The mass, momentum, and energy conservation of the neutral gas can then be written as

$$\frac{\partial(S\rho)}{\partial t} + \frac{\partial(S\rho u)}{\partial R} = 0$$

$$\frac{\partial(S\rho u)}{\partial t} + \frac{\partial(S\rho u^2)}{\partial R} + S\frac{\partial p}{\partial R} = -SF_{gd}$$

$$\frac{\partial}{\partial t}\left(\frac{1}{2}S\rho u^2 + \frac{1}{\gamma-1}Sp\right) + \frac{\partial}{\partial R}\left(\frac{1}{2}S\rho u^3 + \frac{\gamma}{\gamma-1}Spu\right) = S(Q_{ext} - Q_{gd}),$$

where ρ is the gas mass density, p is the gas pressure, u is the gas velocity, R is the radial distance from the center of the nucleus, S is the area function (for spherical geometry $S = R^2$), F_{gd} is the momentum transfer from the gas to the meteoroids, Q_{gd} is the energy transfer rate from the gas to the meteoroids, Q_{ext} is the external heat source (photochemical heating and infrared, thermal cooling), and γ is the gas specific heat ratio.

If we neglect collisions between individual meteoroids, it is possible to write the equation of motion for an individual meteoroid in a radially expanding coma as (cf. Weigert, 1959)

$$\frac{dv}{dt} = \frac{C_D}{2}\frac{A}{m}\rho(u-v)^2 - \frac{Gm_n}{R^2},$$

where v is the meteoroid velocity, C_D is the drag coefficient (see Probstein, 1969, and Gustafson, 1994, for discussion), A/m is the meteoroid cross-section to mass ratio, and m_n the nucleus mass. The first term on the right hand side is the acceleration of the meteoroid due to the gas drag, and the second term is the gravitational attraction from the cometary nucleus.

In the presence of an external radiation field, the energy balance equation for a meteoroid is (Probstein, 1969)

$$C\frac{dT}{dt} = 4\frac{A}{m}q_{gd} + \frac{A}{m}\epsilon_{abs}J_R - 4\frac{A}{m}\epsilon_{em}\sigma_{SB}T^4,$$

where C is the meteoroid specific heat, T is the meteoroid surface temperature, q_{gd} the gas-meteoroid heat transfer rate per unit surface area, J_R is the radiation energy flux at cometocentric distance R, ϵ_{abs} and ϵ_{em} are the meteoroid absorption and infrared emission emissivities, respectively. Finally, the dust size distribution function, $f(m)$, obeys the following continuity equation:

$$\frac{d[Sf(m)]}{dt} = \frac{z(t)}{m}\delta(R-R_n),$$

where $z(t)$ is the meteoroid production rate per unit surface area of meteoroids with mass m, and δ is the Dirac-function. The last equation implicitly assumes that a released meteoroid does not contain sublimating ices or fragment.

The meteoroids decouple from the gas at a distance of (e.g., Keller, 1983) $\sim 30R_n$. The distance, R_{GS}, at which the meteoroid is no longer influenced by the gravitational attraction is usually denoted the "sphere of influence." There are, however, several definitions of the "sphere." We adopt that of Öpik (1963), $R_{GS} = r[m_n/(2M)]^{1/3}$, where r is the heliocentric distance, m_n and M are the mass of the nucleus and the Sun respectively. At $r = 1$ AU, and assuming the bulk density of the nucleus to be 0.6 g cm^{-3}, we find that $R_{GS} \sim 100R_n$.

As pointed out in chapter 2, Crifo (1991) question the validity of the "classical hydrodynamical" models, when computing the terminal meteoroid velocities. The models are based on the assumptions that the meteoroids are, e.g., spherical and of equal densities.

Further, the P/Halley observations show discrepancies, for both large and small meteoroids, when compared to the "classical hydrodynamical" models. Therefore, we chose to use observations to estimate the upper limit to the ejection velocity, and follow Gustafson (1989b). Gustafson used the gas flow velocity, v_{max} (km sec^{-1}), at distance r (AU) from the Sun, approximated by the empirical relation (Malaise, 1970; Delsemme, 1982)

$$v_{max} = 0.58 r^{-0.5},$$

as the upper limit to the meteoroid ejection.

Collisions

The dynamics involved in the collision process is extremely complex. The outcome of the collision depends on several parameters, e.g., shape, density, strength of both projectile and target, impact velocity, impact geometry and target spin rate. In this section we describe the dynamics of the meteoroid, after the collision, but before it is completely left to interplanetary forces.

Radiation forces, which are discussed in the next section, start to act on the meteoroid as soon as it leaves the parent body. As the meteoroid leaves the parent body it is necessary that the ejection velocity, v_{ej}, is larger than the escape velocity, v_{esc}. If $v_{ej} < v_{esc}$, the meteoroid will fall back onto the parent. Assuming a parent body of mean radius R (km) and average density of $\approx$ 2.5 g cm^{-3}, it is possible to estimate the escape velocity as $v_{esc} \approx R$ m sec^{-1}.

To determine when the meteoroid is no longer influenced by the gravitational attraction from the parent body, it is customary to use the concept of the sphere of influence.

Following the calculations in the preceding section (based on Öpik's (1963) definition, with r = 2.5 AU), we find that the sphere of influence is located at a distance of $\approx 400R$.

As an upper limit to the ejection velocity we use

$$v_{max} = 400\ m\ \sec^{-1}.$$

This ejection velocity might reasonably result from a collision between asteroids in the asteroid belt. The relation is used in chapter 4, when the ejection condition for a genetic relation is developed. The upper velocity limit for collisions used here, is comparable to the upper limit assigned to cometary activity (see preceding section), at the inner edge of the asteroid belt.

Interplanetary Space

The theory investigating the motion of bodies in interplanetary space - celestial mechanics - traditionally refers to the gravitational N-body problem, and can be described in terms of Hamiltonian mechanics (e.g., Brouwer & Clemence, 1961). As long as the large bodies - such as the planets - are considered, this "clean," conservative formalism is astonishingly accurate.

However, comet P/Encke showed deviations from the theory, owing to the non-gravitational thrust from ejected material (Whipple & Sekanina, 1979). Even the Moon shows deceleration in its orbit that cannot be explained through gravitational influence from the Sun or the planets; the orbital energy is dissipated through tides raised in the Earth's seas. The interplanetary orbit of a meteoroid is much more affected by non-gravitational perturbations than a comet or the Moon (for a review on non-gravitational perturbations on meteoroids, see Burns et al., 1979; Gustafson, 1994).

The term perturbation needs some clarification. The two-body or Keplerian motion, describing the motion of two point-masses revolving around each other, has an analytical solution (found by Isaac Newton as he derived Kepler's three laws). Adding a third body has the effect of rendering the equations of motion non-integrable, requiring numerical approximations. However, the motion of interplanetary bodies in the Solar System, e.g., the orbits of planets, comets, and meteoroids around the Sun or moons around a planet, is to first approximation described through the Keplerian motion. Any deviations from Keplerian motion, due to, for example, planets attracting each other and the Sun or the thrust on a comet through cometary activity, are investigated under the theory of perturbations. Perturbations are further categorized as gravitational (a third or more bodies enter into the equations of motion, and are in the Solar System called planetary perturbations) or non-gravitational (e.g., sunlight radiation forces).

The solar gravitational force $\vec{F}_g$ (vector) dominates on meteoroids larger than ~ 1 μm (Gustafson, 1994), and all perturbations are therefore measured against it. Isaac Newton showed that the motion of bodies in the Solar System is governed by an inverse square law;

$$\vec{F}_g = -\frac{GMm}{r^2}\hat{r},$$

where G is the universal constant of gravitation, M the solar point mass, m the mass of the meteoroid where it is assumed that $m \ll M$, and $\hat{r}$ is the unit heliocentric radius vector. To compare different forces acting on a meteoroid, it is instructive to investigate their dependence on the characteristic size, s, of the meteoroid. The gravitational force is proportional to the volume (s^3) of the meteoroid.

Here we need to point out that only the gravitational and the radiation pressure force are important for the dynamical evolution of the meteoroids (s larger than ≈ 500 μm) and the time scales considered (≈ 10^4 years). Nevertheless, for completeness we include discussion on other, less important forces acting on the meteoroid in interplanetary space.

There are several perturbing forces acting on a meteoroid (forcing the orbit to deviate from Keplerian motion). The aim here is to evaluate which of these forces that are important for the orbital evolution of meteoroids, and find expressions to incorporate into the equations of motion. The forces considered are; sunlight radiation forces, solar wind corpuscular forces, solar wind Lorentz forces, and forces due to the spin of the meteoroid.

The force due to sunlight radiation acting on a meteoroid can be separated into two parts (Burns et al., 1979; Gustafson, 1994); (1) the primary radiation pressure force, which partially cancels the solar gravity, and (2) the second-order Poynting-Robertson light drag, which slowly dissipates the orbital energy of the meteoroid, forcing it to slowly spiral towards the Sun.

The sunlight radiation pressure force, $\vec{F}_r$, is usually the second strongest (second to solar gravity). The force is written as;

$$\vec{F}_r = \frac{S_0 A Q_{pr}}{r^2 c} \hat{r},$$

where S_0 is the solar insolation at 1 AU, A the cross-section of the meteoroid, c the velocity of light, and Q_{pr} the efficiency factor for radiation pressure (van de Hulst, 1957; Gustafson, 1994). Note that the radiation pressure force is proportional to the surface (s^2) of the meteoroid.

Both the radiation pressure force and the gravitational force have an inverse square law dependence on heliocentric distance. The magnitude of the radiation pressure force to gravity ratio, β, is independent on heliocentric distance, and is found to be

$$\beta = C_r Q_{pr} (A/m),$$

where $C_r = 7.6 \times 10^{-5}$ g cm^{-2} (Gustafson, 1989a). For sufficiently large meteoroids ($s \approx 10$ μm), it is found that $\beta \propto s^{-1}$, implying that the importance of radiation pressure diminishes with meteoroid size. From the definition of β, it is seen that radiation pressure from sunlight partially cancels solar gravity, with a factor $1 - \beta$. Further, if $\beta \geq 1$, the meteoroid will escape the Solar System, but for the meteoroids considered in this thesis (those generating photographic meteors), $\beta < 1$ is always satisfied.

The Poynting-Robertson light drag is due to the orbital motion, at speed v, of the meteoroid around the Sun. The drag is caused by the non-isotropic re-emission of radiation absorbed by the meteoroid. The formal derivation of the radiation forces (where the radiation pressure force is one part) requires special relativity (Robertson, 1937; Burns et al., 1979; Klačka, 1992). To first order in v/c, not requiring special relativity since it is then only an abberation effect, the radiation forces acting on a spherical meteoroid is

$$|\vec{F}_g| \beta [(1 - 2\dot{r}/c)\hat{r} - (r\dot{\theta}/c)\hat{\theta}],$$

where the unit vector $\hat{\theta}$ is normal to $\hat{r}$ in the orbital plane. The velocity independent radial term is the radiation pressure force discussed above. The second term along $\hat{r}$, and the transverse last term is referred to as the Poynting-Robertson light drag. We note that the Poynting-Robertson light drag is a second-order effect, since $v/c < 1$, compared to the radiation pressure force, and that the drag decreases with the meteoroid size.

The solar wind corpuscular forces are analogous to the solar radiation forces. The solar wind consists of a hot plasma of ionized gas - electrons, protons, and alpha-particles - coupled to the interplanetary magnetic field. Of the species in the solar wind, it is the proton momentum flux which is most important to meteoroid dynamics.

The ratio of the proton pressure force (which has an inverse-square dependence on heliocentric distance) to solar gravity is (Gustafson, 1994)

$$\beta_{sw} = C_p(A/m),$$

where $C_p \approx 3.6\times10^{-8}$ g cm^{-2}. The ratio of proton to radiation pressure (with $Q_{pr} = 1$) is $\approx 5\times10^{-4}$. Solar wind corpuscular pressure is negligible compared to sunlight radiation pressure. However, this does not mean that the corpuscular drag is negligible compared to Poynting-Robertson drag.

As previously mentioned, solar wind corpuscular forces are analogous to radiation forces, and can be represented as (Klačka, 1992; Gustafson, 1994)

$$|\vec{F}_g|\beta_{sw}[(1-2\dot{r}/v_{sw})\hat{r} - (r\dot{\theta}/v_{sw})\hat{\theta}],$$

where v_{sw} is the solar wind speed, assumed to be independent of heliocentric latitude and distance. The corpuscular to Poynting-Robertson drag ratio, assuming the solar wind speed to be 500 km sec^{-1} (a rough average over slow and fast solar wind), is $(\beta_{sw}/v_{sw})(c/\beta) = 0.3$, and this value is used throughout the thesis.

The solar wind Lorentz force is proportional to the interplanetary magnetic field(inversely proportional to heliocentric distance), the velocity with which the meteoroid moves relative to the field, and the charge of the meteoroid. The Lorentz force is approximately equal to solar gravity and the sunlight radiation pressure force for a 10^{-1} μm

particle at 1 AU. The Lorentz force is proportional to the linear dimension, s, of the meteoroid. Since the radiation pressure force is proportional to the area (s^2), it is safe to ignore the solar wind Lorentz force on meteoroids larger than 1 μm (Gustafson, 1994). This holds true within 1 AU, but further out in the Solar System, where the interplanetary magnetic field is falling off only inversely proportional with heliocentric distance, this size becomes larger. Still, for the sizes of the meteoroids and their heliocentric orbits (with aphelion distance within Jupiter's orbit) considered here, the Lorentz force is negligible.

If a meteoroid is spinning sufficiently rapidly (or is large enough compared to its spin period), it will not be in thermal equilibrium; the evening hemisphere will emit more momentum than the morning hemisphere, due to the temperature difference between them (e.g., Peterson, 1976; Burns et al., 1979; Gustafson, 1994). Depending upon the orientation of the spin axis relative to the meteoroid Sun direction, the net momentum force can result in either an accelerative or a drag force, termed the Yarkovsky effect. According to Öpik (1951), this process was first describe around 1900 by I. O. Yarkovsky, in a pamphlet whose reference has been lost.

The Yarkovsky effect is dependent on several parameters; the density, heat capacity, and thermal conductivity of the material, the spin rate and the orientation of the spin axis, and the morphology of the meteoroid. These parameters can presently not be estimated directly from observed meteor data.

The ratio of the Yarkovsky effect to the Poynting-Robertson light drag is proportional to meteoroid size and is inversely proportional to heliocentric distance. The two effects are approximately equal on a meteoroid of 1 cm at 1 AU. However, for meteoroids of that size or larger, both effects are small compared to the uncertainties in the meteor data, when

integrations are made only 10^4 years back in time (a nominal value for the meteoroids treated in this thesis).

The Yarkovsky effect is not included into this thesis. However, it should be borne in mind that it may be important, but at the present time we can not estimate the parameters involved.

We are now ready to present the full system of equations of motion in the heliocentric system:

$$\ddot{\vec{r}}_i = -G(M+m_i)\frac{\vec{r}_i}{r_i^3} + \sum_{k=1,k\neq j}^{N} Gm_k\left(\frac{\vec{r}_k-\vec{r}_i}{|r_k-r_i|} - \frac{\vec{r}_k}{r_k^3}\right), \quad i=1,\ldots,N$$

$$\ddot{\vec{r}} = -GM(1-\beta)\frac{\vec{r}}{r^3} - GM\frac{\beta_{r+sw}}{r^2}\left[\left(\frac{\vec{r}\cdot\vec{v}}{rc}\right)\frac{\vec{r}}{r} + \frac{\vec{v}}{c}\right] + \sum_{k=1}^{N} Gm_k\left(\frac{\vec{r}_k-\vec{r}_i}{|r_k-r_i|} - \frac{\vec{r}_k}{r_k^3}\right),$$

where the first N equations describe the motion of the planets (where the Earth-Moon system is given a barycentric representation), and the last equation describes the motion of the meteoroid. The parameter $\beta_{r+sw} = 1.3\beta$, accounts for the solar wind corpuscular forces.

No general relativistic corrections are made to the equations of motion. These corrections are negligible compared to the uncertainties in the meteor data.

Catastrophic meteoroid collisions in interplanetary space under the time span considered ($\approx 10^4$ years) may be important. Figure 3-1 shows the catastrophic collisional life times, τ_c, as a function of heliocentric distance. These life times are estimated from the interplanetary flux model and the assumptions used by Grün et al. (1985). We note that a meteoroid of 1 g has a catastrophic collisional life time of roughly 10^4 and 20 years at a heliocentric distance of 1 and 0.1 AU, respectively.

Atmospheric Flight

As the meteoroid approaches the Earth, it is subject to additional perturbations. The largest perturbation is due to the Moon. At the distance of six times the semi-major axis of the Moon's orbit around the Earth, we use a separate treatment of the Earth and the Moon (the absolute fractional difference in acceleration between a separate and a barycentric representation is then less than 10^{-3}). This corresponds to adding one more equation of motion, analogous to that of the other planets, for the Moon. At the distance of ≈ 42,000 km from the Earth's center (approximately geosynchronous orbit), the perturbation due to the Earth's oblateness is equal to the perturbation due to the Moon. At the top of the Earth's atmosphere (here taken as 150 km) the perturbation due to the Earth's oblateness is ≈ 10^{-3} of the Earth's monopole acceleration. The Earth's oblateness is not accounted for in this thesis.

As the meteoroid enters the Earth's shadow, no radiation forces act on the meteoroid (Gustafson & Adolfsson, 1996). This corresponds to setting β and $\beta_{r,sw}$ to zero in the meteoroid's equation of motion.

From the top of the atmosphere (150 km), down to the first point of recorded light (meteor beginning height), we neglect mass-loss. The equation of motion is then

$$\frac{dv}{dt} = -\frac{C_D}{2}\frac{A}{m}\rho v^2 + \cos z_R \frac{GM_E}{(R_E+h)^2},$$

where v is the speed of the meteoroid, C_D the drag coefficient, ρ the air density, z_R the zenith distance, M_E and R_E the mass and the radius of the Earth, and h the height in the atmosphere. The first term on the right hand side is due to atmospheric drag and the second term is due to the Earth's gravitation. Note the similarity between this equation of motion, and

the one describing the motion of a meteoroid in the inner cometary coma (section 3.1). The height in the atmosphere is governed by

$$\frac{dh}{dt} = -v \cos z_R.$$

The simple, but effective, theory describing the motion and ablation of a meteoroid in the Earth's atmosphere was developed during the last part of the nineteenth century, and it was given its present appearance through Hoppe (1937). The theory, called the single-body theory, is described through three equations; the deceleration equation conserving momentum, and the mass-loss equation

$$\frac{dv}{dt} = -\frac{C_D}{2}\frac{A}{m}\rho v^2$$
$$\frac{dm}{dt} = -\frac{\Lambda}{2\xi}A\rho v^3,$$

where Λ is the heat transfer coefficient (fraction of the kinetic energy which goes into ablation of the meteoroid material), and ξ the energy needed to ablate a unit mass of meteoroid material. The third equation, the height equation, is the previous equation determining the height, h, in the atmosphere. It is important to note that the cross-section to mass ratio is once again a key parameter in the dynamics of the meteoroid motion.

Two important parameters in meteor physics are the ablation coefficient σ and the pre-atmospheric velocity v_∞. Dividing the deceleration equation with the mass-loss equation, we obtain

$$\frac{dv}{dt} = \sigma m v \frac{dm}{dt},$$

where

$$\sigma = \frac{\Lambda}{\xi C_D}.$$

Integration of the previous equation yields

$$m = m_\infty \exp[\frac{1}{2}\sigma(v^2 - v_\infty^2)],$$

where the subscript ∞ denotes the pre-atmospheric value of the quantity.

Double-station photographs are the most precise records of meteoroid motion through the atmosphere. For each time mark (defined by the shutter mechanism, interrupting the exposure), the records contain the distance flown by the meteoroid in its trajectory, and the height in the atmosphere. Pecina and Ceplecha (1983; 1984) solved the equations of the single-body theory for observed meteors through the use of a least-squares solution. The authors assumed that the drag coefficient, the heat transfer coefficient, the energy needed to ablate a unit mass material, and the zenith distance remained constant throughout the trajectory. In addition to this they also assumed that the meteoroid remain self-similar during the atmospheric flight.

The output parameters, with associated one standard deviation estimates, of Pecina and Ceplecha's solution are; the pre-atmospheric speed v_∞, the ablation coefficient σ, and the quantity $(C_D/2)(A/m)$. The last parameter, with an assumption of the drag coefficient, gives the pre-atmospheric cross-section to mass ratio of the meteoroid.

In addition to these parameters, the solution also yields the error in distance along the trajectory, σ_l, for one measured point. This quantity is a measure of the magnitude of the residuals to the single-body or gross-fragmentation solution.

There are two main advantages of the method that Pecina and Ceplecha developed; (1) until their method, based on a physical theory, only non-physical interpolation polynomials (Whipple, 1938) had been used to analyze the motion of the meteoroid, and (2) the solution yields estimates of all parameters, accompanied by an estimate of the standard deviation.

Ceplecha et al. (1993) extended the method to account for sudden fragmentation points, and the method is therefore called a gross-fragmentation solution. On photographs it is sometimes possible to locate a fragmentation point, and follow the motion of several fragments. The gross-fragmentation method is capable of identifying the fragmentation point, by minimizing the observed minus computed distance along the trail.

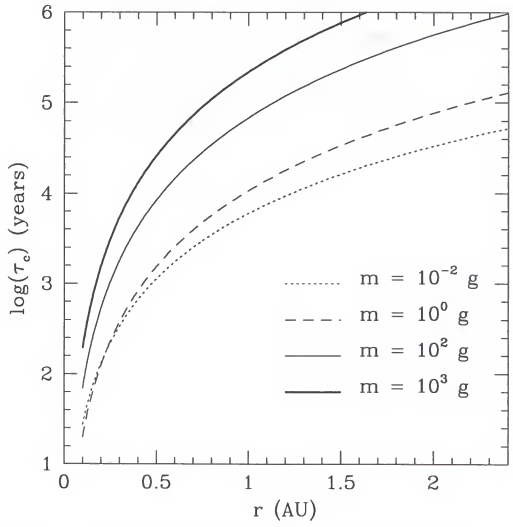

Figure 3-1 Catastrophic collisional time scale for meteoroids in the inner Solar System.

CHAPTER 4
PARENT-DAUGHTER ASSOCIATION METHOD

This chapter describes the method used to establish a quantitative measure of the genetic relation between specific meteoroids and their proposed parent bodies.

The trajectory of the meteoroid separates from that of the parent body. This is due to differences in the forces acting on the meteoroid and the parent, and due to the velocity difference acquired in the ejection process. While the trajectories may intersect later, they usually do so at high relative velocities.

Assume that we have the heliocentric orbits, at the epoch of the observed meteor, for a specific meteoroid and its proposed parent body. How do we establish a genetic relation? The key idea is to search for the ejection point. We follow and extend the work by Gustafson (1989b). He integrated the equations of motion for twenty Super-Schmidt Geminids and their proposed parent body Phaethon, until he identified possible ejection points. The question is, how possible is the ejection point, or, in other words, how may we estimate the probability for a genetic relation?

To answer this question, we need to realize two important aspects of the problem. First, the trajectories of the meteoroid and the parent body are only estimates of their true trajectories; we need to account for the observational errors. Secondly, the trajectories found through numerical integration are sensitive to the initial conditions; the bodies may or may not get trapped in resonances or experience chaotic motion due to small differences in initial conditions. Because of the second aspect, it is not advisable to use only one trajectory to imply

a genetic relationship between a specific meteoroid and its proposed parent body (although the technique may work when we only need a qualitative description of the trajectory evolution).

The Parent-Daughter association method developed in this thesis acknowledges these aspects, and uses them to find the ejection point and estimate the probability of a genetic relation. Several trajectories, sampled from the error distributions in the meteor data, are integrated back in time for each meteoroid. This approach is statistical, and has the advantage that any passage through a resonance, a chaotic orbital region, and uncertainties in the numerical integrations are automatically accounted for.

The use of the Parent-Daughter association method on several meteoroids belonging to the same stream, has the capability of revealing the formation process (cometary activity or collision), and its duration. It is usually anticipated that formation due to cometary activity should occur over several revolutions around the Sun, close to perihelion, and with an ejection velocity vector toward the solar hemisphere. Formation due to collisions would have occurred predominantly in the asteroid belt, where the probability of collisions is high. Generally we would also anticipate that the duration of such an event would be shorter than that for cometary activity. However, these are only probable scenarios, and the best way to find out if they are true, is by using the Parent-Daughter association method.

The box-diagram in figure 4-1 is a schematic outline of the Parent-Daughter association method. The method consists of three separate parts: (1) computation of the distribution of trajectories (as a function of time) for the proposed parent body, (2) computation of the distribution of trajectories (as a function of time) for the meteoroid, and (3) the search for the ejection point through the convolution of the trajectory distributions, and the use of criteria to ensure that the ejection took place under physically realistic conditions.

The title of the thesis contains the words dynamic and probabilistic. The word dynamic refers to the use of the integration of the equations of motion, and the word probabilistic refers to the sampling in the error distributions.

Sampling of Error Distributions and Orbital Integrations

It is assumed that the single-body or the gross-fragmentation solution to the meteor data removes all systematic effects, leaving only observational errors. It is further assumed that the errors obey a normal (or Gaussian) probability distribution.

To ensure that the sampling generates a normal probability distribution, the number of samples is set to 50. The normal deviates are computed through the transformation of a random deviate with a uniform probability distribution (Press et al., 1992).

It is also possible to generate a normal probability distribution through weighing of the sampled values. Assume that an input parameter, e.g., the meteoroid cross-section to mass ratio, is chosen at equidistant values from the estimated true value. Each value is then given a weight such that the weights sum up to unity. However, a problem may then arise. Since the trajectory evolution back in time is sensitive (small change in the value may give large differences in the trajectories) to the input values, it may be that some equidistant values give trajectories which are not representative of the distribution. These trajectories are then given too high a weight and probability.

A random sampling, i.e., no rule for selecting the samples, of the values avoids this problem. Moreover, it is easier to improve the statistics if random sampling is used; just draw more samples.

Meteoroids

This subsection follows the steps used in the computer code. It is assumed that the velocity (direction and magnitude) and the cross-section to mass ratio, with their associated error estimates, are already computed (see chapter 5 for details of these computations) at the point of first recorded light (the meteor beginning height).

The first step is to sample the four input parameters; the speed, v, the right ascension, α, the declination, δ, and the cross-section to mass ratio, A/m, of the meteoroid.

All computations are made in the ecliptic system J2000.0. We precess the radiant (right ascension and declination in the equatorial coordinate system) to J2000.0. The transformation used (Astronomical Almanac, p. B19) is

$$
\begin{aligned}
T' &= (T-2000.0)/100.0 \\
M &= 1.2812323\,T' + 0.0003879\,T'^{2} + 0.0000101\,T'^{3} \\
N &= 0.5567530\,T' - 0.0001185\,T'^{2} - 0.0000116\,T'^{3} \\
\alpha_m &= \alpha - 0.5(M + N\cos\alpha\tan\delta) \\
\delta_m &= \delta - 0.5\,N\cos\alpha \\
\alpha' &= \alpha - M - N\sin\alpha_m\tan\delta_m \\
\delta' &= \delta - N\cos\alpha_m
\end{aligned}
$$

where T is the epoch of the meteor, α' and δ' are precessed to J2000.0, and all angles are in degrees.

The classical way (Whipple & Jacchia, 1957) of estimating the orbital elements of a meteoroid is based on a number of corrections, in analytical form, to the observed meteor velocity. The classical treatment involves two regions where systematic errors are introduced. The first region is where the atmospheric drag (most important deep down in the atmosphere) is comparable to the Earth's gravitational acceleration (most important high up in the

atmosphere). The second region is where the gravitational influence of the Sun becomes important relative to the gravitational influence of the Earth. These deficiencies of the classical method were pointed out by Pecina (1989; 1994).

The classical, approximate treatment was developed when no computers were available. Today, when computers are common, there is no reason not to use a complete integration scheme, from the height at first point of first light, through the two regions previously discussed, out into interplanetary space. One should, however, not forget the merits of an analytic, approximate method; it yields insight into the physics of the problem (where a numerical treatment may not), and it serves as a test for a more elaborate, numerical computation.

We adopt Pecina's (1989) suggestion of using a pre-atmospheric velocity at a given height in the atmosphere (v_∞, as strange as it may seem, is not associated with any particular height, rendering the parameter ambiguous, and the assumption of negligible atmospheric drag is not rigorously proven), and chose the height to be 150 km (to ensure that atmospheric drag is small for the meteoroids we investigate). This coincides with the highest point tabulated in the CIRA 1972 monthly atmosphere.

Using the sampled input parameters, the vectorial differential equation of motion for the meteoroid is

$$\frac{d\vec{v}}{dt} = -\frac{C_D}{2}\frac{A}{m}\rho v\vec{v} - GM_E\frac{\vec{r}_E}{r_E^3},$$

where $r_E = R_E + h$ is integrated from the height of first recorded light to the height 150 km, and we use the CIRA 1972 monthly atmosphere for the air density ρ. The velocity, $\vec{v}_{150}$, is now pre-atmospheric.

The velocity, corrected for diurnal abberation (e.g., Whipple & Jacchia, 1957) is

$$\vec{v}_{150,C} = \vec{v}_{150} + \frac{2\pi}{T_s} r_E \, (\cos\phi\sin\theta, \cos\phi\cos\theta, 0)^T,$$

where T_s is the sidereal period of rotation of the Earth is seconds = 86,164, r_E the geocentric distance, ϕ the geocentric latitude, and θ the sidereal time at the epoch of the meteor.

All integrations in interplanetary space are made in the heliocentric ecliptic coordinate system. To transform from the equatorial coordinate system (in which the radiant, right ascension and declination, is defined) we use the following transformation matrix;

$$\bar{R}(\epsilon) = \begin{matrix} 1 & 0 & 0 \\ 0 & \cos\epsilon & \sin\epsilon \\ 0 & -\sin\epsilon & \cos\epsilon \end{matrix},$$

where ϵ is the obliquity, at epoch T, of the ecliptic, computed as (Astronomical Almanac, p. B18)

$$T' = (T-2000.0)/100.0$$
$$\epsilon = 23.43929111 - 0.013004167\,T' - 0.0000001653\,T'^2 + 0.0000005036\,T'^3.$$

All major planets (with the Earth and the Moon in a barycentric representation), except Pluto, with starting elements (J2000.0) from the Astronomical Almanac (p. E3), are integrated to the epoch of the meteor.

The position and the velocity, with respect to their barycentre, of the Earth and the Moon, at the epoch of the meteor, is computed according to the Astronomical Almanac (p. D46). The increments in position and velocity for the Earth, are also applied to the meteoroid.

Before we start the integrations back in time from the atmospheric height 150 km, we need to estimate the value of β, the radiation pressure force to solar gravity ratio. From meteor data (see chapter 5) we find the pre-atmospheric quantity $(C_D/2)(A/m)$. In chapter 3 it is found that $\beta = C_r Q_{pr}(A/m)$. This means that to estimate β, we first have to estimate the drag coefficient C_D and the efficiency factor for radiation pressure Q_{pr}.

Rigorous computations of the drag coefficient for various shapes and flow conditions (ranging from free-molecular to continuous flow) are extremely difficult (Bronshten, 1983). Because of this we adopt the customary value $C_D = 2$, corresponding to free-molecular flow (air-molecules only interact with the meteoroid, not among themselves) for a sphere.

The photographic meteoroids we consider are large enough, and opaque to sunlight, so that the large particle approximation and geometric optics apply (Gustafson, 1994). The optically large meteoroids have Q_{pr} values that are strictly independent of the meteoroids shape when averages are made over random orientations (Gustafson, 1989a), as long as they are convex in shape. We can therefore chose any convex shape when we evaluate Q_{pr}. This is done, using geometric optics for a sphere of albedo w (fraction of reflected to incident radiation), where $Q_{pr} = 1 - wg$ (van de Hulst, 1957). The geometrical factor g is inside the interval from unity (for totally forward scattering meteoroids) to -1 (for total back-scattering). Q_{pr} is close to unity at the small albedo of typically a few percent for cometary and asteroidal chondritic material, and we therefore adopt $Q_{pr} = 1$.

Radiation pressure on a meteoroid vanishes as the meteoroid enters the Earth's shadow. Therefore, as we integrate the motion of the meteoroid from the top of the atmosphere into interplanetary space, we account for radiation pressure ($\beta > 0$) when the meteoroid leaves the Earth's shadow. We do not account for the penumbra (partial solar eclipse) effect.

The finite radiation pressure force will mostly affect the semi-major axis and the eccentricity. For meteoroids observed at the Earth's orbit, the semi-major axis will always increase with β, and the eccentricty decreases with β if the semi-major axis is less than 1 AU, and increase otherwise (Gustafson & Adolfsson, 1996).

Second-order effects, the Poynting-Robertson light drag and the solar wind corpuscular force, also start to act when the meteoroid leaves the Earth's shadow ($\beta > 0$). This is done although the solar wind corpuscular force only acts as the meteoroid is outside the Earth's magnetosphere.

We switch to a barycentric representation of the Earth-Moon system, as the distance between the meteoroid and the Earth-Moon barycentre is larger than six times the semi-major axis of the Moon's orbit around the Earth.

The orbit of the meteoroid is sampled every fifth year. This is a compromise; smaller time steps would require too much disk-space on the computer (considering at least 50 sampled trajectories with an integration time of $\approx 10^4$ years), and with larger time steps one may "miss" important sections of the trajectory evolution. Moreover, if one considers the sampled trajectories as time-series, it is possible to Fourier analyze these, and investigate the importance of periodic perturbations by major planets. Since the critical sampling of a sine wave is two sample points per cycle, and the most important perturber in the solar system is Jupiter, with a period of 11.46 years, a time-step of five years is nearly optimum.

We do not store orbital elements, but the position and velocity vectors (corresponding to six double precision numbers) in the heliocentric ecliptic (J2000.0) coordinate system. Orbital elements are easily computed through well-known expressions (e.g., Brouwer & Clemence, 1961).

Parent Bodies

In general, the uncertainties in the orbital elements for a parent body are much smaller than for a meteoroid. This means that it is better to invest computing time into the meteoroid trajectories, than into the parent body trajectories. However, since the evolution of the trajectories is sensitive to the input values to the equations of motion, it is advisable to sample more than one orbit of the parent body.

Muionen and Bowell (1993) use Post-Bayesian probability theory to estimate the orbital elements and the one standard deviation error associated with these quantities. Further, their method makes it possible to detect non-gravitational forces acting on the body.

It has been known for a long time that comets have non-gravitational perturbations affecting their motion, the prime example being comet P/Encke. Whipple (1950b; 1951), in his famous icy conglomerate model for the cometary nucleus, was able to explain several features of comets. Among these features was the observed perturbations to comet trajectories, which he explained as a rocket-like effect due to the outgassing of material. In the remaining of this subsection we describe how to account, in terms of the equations of motion, for the non-gravitational accelerations of parent bodies.

Efforts have been made to model the non-gravitational accelerations with empirical terms in the comets' equation of motion (see, e.g., Yeomans, 1994). Marsden et al. (1973) introduced the standard, or symmetric, non-gravitational model for cometary motions: a rapidly spinning cometary nucleus is assumed to undergo vaporization from water snow that acts symmetrically with respect to perihelion. The equation of motion is written as

$$\ddot{\vec{r}} = -GM\frac{\vec{r}}{r^3} + \sum_{k=1}^{N} Gm_k\left(\frac{\vec{r}_k - \vec{r}}{|r_k - r|^3} - \frac{\vec{r}_k}{r_k^3}\right) + A_1 g(r)\hat{r} + A_2 g(r)\hat{T},$$

where the $g(r) = \alpha(r/r_0)^{-m}[1+(r/r_0)^n]^{-k}$. If the non-gravitational acceleration is given in AU/(ephemeris day)^2, r_0 = 2.808 AU for water ice (r_0 is the heliocentric distance where re-radiation of solar energy begins to dominate the use of this energy for vaporizing the comet's ices), the normalizing constant α = 0.111262, and the exponents m, n, and k equal 2.5, 5.093, and 4.6142, respectively. The non-gravitational perturbation is represented through a radial term, $A_1 g(r)$, and a transverse term, $A_2 g(r)$. The transverse unit vector, $\hat{t}$, is directed normal to the unit heliocentric vector, $\hat{r}$, in the orbital plane, and in the direction of the comet's motion. A determination of a non-gravitational parameter normal to the orbit plane (A_3) does not generally improve an orbit solution significantly.

A solution of A_1 and A_2 (which may be time dependent, see Sekanina, 1993) for a comet, is based on observations over a recent and short time period (compared to the integration time $\approx 10^4$). Continuation of integrations further back in time than observations have been made, are therefore subject to a probabilistic treatment. We may view the time dependence and the magnitude of A_1 and A_2 as input parameters to the Parent-Daughter association method.

The trajectories of the proposed parent body are sampled at identical epochs, i.e., every fifth year, as the sampled epochs of the meteoroid trajectories.

Intersection Condition

Unfortunately, the uncertainty in the orbital period of the meteoroid, is so large that knowledge on the position of the meteoroid along its orbit, is lost in just a few orbits around the Sun (Gustafson, 1989b). We therefore do not search for a time and point in space where the meteoroid's location coincides with the location of the presumed parent body. However, in the case where the ejection point occurred quite recent, the coincidence criterion may be used.

Following Gustafson (1989b), we use the second best dynamic criterion for a genetic relation; orbital intersections.

Orbits intersect along their mutual line of nodes. In the singular case (which is rather unlikely to occur in the numerical computations, due to double precision real numbers), where the two trajectories have coinciding orbital planes, all lines in the orbital plane are treated as lines of nodes. The following computations of the location of the mutual nodes, and the distance between the orbits at the mutual nodes, are made according to Greenberg (1981).

Consider the two different trajectories of the parent body (denoted by subscript p) and the meteoroid; semi-major axis (a and a_p), eccentricity (e and e_p), inclination (i and i_p), longitude of ascending node (Ω and Ω_p), and argument of perihelion (ω and ω_p). The positions of the mutual nodes (u and u_p), measured from the ecliptic nodes of the two bodies, are given through

$$\begin{aligned} u_p &= \arctan[-\sin\Delta\Omega/(\cot i \sin i_p - \cos\Delta\Omega\cos i_p)] \\ \cos u &= \cos u_p \cos\Delta\Omega + \sin u_p \sin\Delta\Omega \cos i_p \\ \sin u &= \sin u_p \sin i_p / \sin i, \end{aligned}$$

where $\Delta\Omega = \Omega - \Omega_p$. The first equation yields two values of u_p, 180° apart. Once one of these is selected, the remaining two equations define a unique value of u. The distance, D, between the trajectories at their mutual nodes is computed as

$$D = \frac{a(1-e^2)}{1+e\cos(u-\omega)} - \frac{a_p(1-e_p^2)}{1+e_p\cos(u_p-\omega_p)}.$$

Note that D is defined as the distance of the meteoroid trajectory from the parent trajectory, along the line of nodes. Further, D does not have to be the shortest distance between the two trajectories.

As the distance $D(t)$ (at epoch t) changes sign, and because $D(t)$ is a continuous function over time, the trajectories must have intersected at least once during the time-step, Δt. The intersection condition is then fulfilled if $D(t)D(t+\Delta t) < 0$.

Ejection Condition

The relative velocity, $\vec{v}_{rel}$, between the two trajectories is computed as $\vec{v}_{rel} = \vec{v} - \vec{v}_p$, where $\vec{v}$ is the velocity of the meteoroid, and $\vec{v}_p$ is the velocity of the parent body. The relative speed at intersection, v_{rel}, is the magnitude of $\vec{v}_{rel}$, the heliocentric distance at intersection, r_p, is the magnitude of $\vec{r}_p$, the true anomaly at intersection is $f_p = u_p - \omega_p$, and the direction of the relative velocity with respect to the parent body Sun line is $\alpha = \arccos(-\vec{v}_{rel} \cdot \vec{r}_p)/(v_{rel} r_p)$.

However, none of the quantities computed in the previous paragraph are at the intersection point, since they are computed at two epochs, before and after the intersection occurred. To overcome this problem one could use a numerical approach by using a shorter time-step, Δt, than five years. An analytical approach is difficult, since D depends on ten orbital elements (five for each trajectory), in a highly complicated manner. Instead we use a fast, approximate solution to this dilemma.

The quantities are computed through weighing by the distance between the trajectories, D, such that the weight of the quantity is large when the distance is small, according to

$$<A, D(t)> = \frac{A(t)/D^2(t) + A(t+\Delta t)/D^2(t+\Delta t)}{1/D^2(t) + 1/D^2(t+\Delta t)},$$

where A is any of the scalar quantities we search for. Following this formalism, we compute the estimates

$$v_I = \langle v_{rel}, D(t) \rangle$$
$$r_I = \langle r_p, D(t) \rangle$$
$$f_I = \langle f_p, D(t) \rangle$$
$$\alpha_I = \langle \alpha, D(t) \rangle$$
$$T_I = \langle t, D(t) \rangle,$$

where subscript I denotes the intersection point, and T_I is the epoch of intersection.

The relative speed at intersection v_I, weighted according to the above procedure, is then compared to the upper limit of ejection velocity (from cometary activity or collisions), $v_{\max}$ (estimated in chapter 3), through the ratio

$$R_I = \frac{v_I}{v_{\max}}.$$

The ejection condition is satisfied if $R_I \leq 1$.

Probability Computations

The previous sections, developing the intersection and ejection conditions, treated only two trajectories; one for the parent body and one for the meteoroid. However, the method should be capable of accounting for all sampled trajectories. In order to find an estimate for the probability of a genetic relation we need to account for all, both meteoroid and parent body, sampled trajectories.

The estimated probability, P, of a genetic relation between the meteoroid and the proposed parent body is computed over a time span, e.g., from epoch t_1 to epoch t_2. Consider the extreme (and unrealistic) case where the trajectories of the meteoroid and the parent body are known to 100%, i.e., no uncertainties in the observations and the subsequent numerical

modeling of the equations of motion exist. In that case, we only need to sample two trajectories, since they are completely known. Applying the intersection and ejection conditions, which in this thought example are satisfied, to the two trajectories then gives the estimated probability of a genetic relation as 100%, and the epoch at which ejection took place is only one number.

However, the use of real observations in the sensitive equations of motion, requires that we quote an estimate of the probability for a genetic relation over a time span, since the trajectory distributions usually intersect and cross each other over a much longer time period than the sampling time step in the integrations.

Assume that we have sampled N meteoroid trajectories and M parent body trajectories. Let us investigate the probability that the ejection took place between the epochs t_1 and t_2 ($= t_1 + n\Delta t$, where n is a whole number). We then have to investigate the intersection and ejection conditions for all $N \times M$ possible combinations of the meteoroid and the parent body trajectories, at n different epochs (t_1, $t_1+\Delta t$, ..., $t_1+(n-1)\Delta t$).

Consider that we have the i th meteoroid trajectory and the j th parent body trajectory. We start at epoch t_1 by evaluating the intersection condition $D(t_1)D(t_1+\Delta t) < 0$. If the intersection condition is satisfied, we compute $v_{I,ij}$, $r_{I,ij}$, $f_{I,ij}$, $\alpha_{I,ij}$, and $T_{I,ij}$. We then proceed to evaluate the ejection condition $R_{ij} = v_{I,ij}/v_{\max} \leq 1$. If the ejection condition is satisfied, we define the probability $P_{ij} = 1/(NM)$. If any of the conditions had not been satisfied, $P_{ij} = 0$. Further, assume that we find the ejection condition, R_{ij}, still for the i th and the j th trajectories, to be smaller at a later epoch t_3 ($t_1 < t_3 < t_2$), i.e., $R_{ij}(t_3) < R_{ij}(t_1)$. We then chose to use $v_{I,ij}$, $r_{I,ij}$, $f_{I,ij}$, $\alpha_{I,ij}$, and $T_{I,ij}$ computed at t_3.

Once we have made the previous computations for all $N \times M$ possible combinations. The estimated probability of a genetic relation, P, between the meteoroid and the proposed

parent body during the time span from t_1 to t_2, is computed as

$$P = \sum_{i=1}^{N} \sum_{j=1}^{M} P_{ij}.$$

The quantities describing the conditions at the ejection point are estimated as

$$\bar{x} = \frac{\sum_{i=1}^{N} \sum_{j=1}^{M} P_{ij} x_{ij}}{\sum_{i=1}^{N} \sum_{j=1}^{M} P_{ij}},$$

with a standard deviation

$$\sigma(\bar{x}) = \sqrt{\frac{\sum_{i=1}^{N} \sum_{j=1}^{M} P_{ij} (\bar{x} - x_{ij})^2}{(\sum_{i=1}^{N} \sum_{j=1}^{M} P_{ij}) - 1/(NM)}},$$

where x can be R_I, v_I, f_I, α_I, and T_I, or any other quantity defined at the intersection.

One problem arise when we compute $\bar{x}$. Consider the case where both nodes (180° apart) satisfy the criteria for a genetic relation, between the two epochs t_1 and t_2. This has the effect that, e.g., the true anomaly, $\bar{f}_I$, is estimated to be in between the two values at the nodes. To avoid this problem, we compute the conditions of ejection, i.e., probability, relative velocity, etc., for both nodes, and present them separately (see chapter 7).

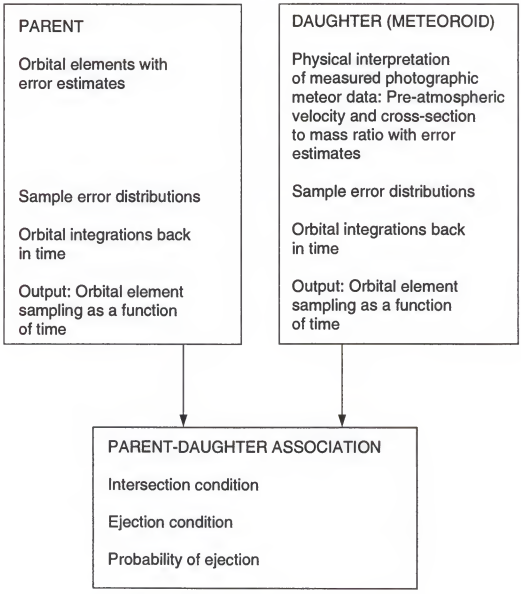
PARENT
Orbital elements with error estimates
Sample error distributions
Orbital integrations back in time
Output: Orbital element sampling as a function of time
DAUGHTER (METEOROID)
Physical interpretation of measured photographic meteor data: Pre-atmospheric velocity and cross-section to mass ratio with error estimates
Sample error distributions
Orbital integrations back in time
Output: Orbital element sampling as a function of time
PARENT-DAUGHTER ASSOCIATION
Intersection condition
Ejection condition
Probability of ejection

Figure 4-1 Box-diagram of the Parent-Daughter association method.

CHAPTER 5
OBSERVATIONAL MATERIAL AND DATA REDUCTION

Meteoroids

Several different techniques are used to detect a meteor, which imply the existence of a meteoroid. Faint, low-mass meteors are detected through the use of radar techniques (e.g., Baggaley & Taylor, 1992). Ablated and ionized meteoroid material forms a column of ions and electrons, trailing the meteoroid in its atmospheric trajectory. Electrons in the column reflect the emitted radio-waves, which are detected with antennas. Recombination of electrons produce radiation, detected through photographic techniques. The most widely used technique, is that of photographing the meteor with two or more cameras at different locations. In addition to these techniques, meteors ar also detected with the aid of TV-equipment (e.g., Hawkes, 1993).

Double-station photographs of a meteor gives the most precise meteor data - distance along the trail, height in the atmosphere, and intensity of the radiation for each time mark. An interrupting shutter defines the time marks. The observations define the (nearly) straight-line trajectory of the meteor as the intersection of two planes. Each plane is defined by one station and the projected view of the trajectory as seen against the star background from that station. Ideally, there are as many measured points along the trajectory, as there are interruptions of the meteor trail (for a comprehensive review of reduction of meteor photographs, see Whipple

& Jacchia, 1957). In comparison, a radar observation yields meteor data at only one point; the point of specular reflection from the electrons in the column.

We have chosen to use only the most precise meteor data available. This requirement leaves us with doubly photographed meteors. Further, the Parent-Daughter association method (chapter 4) requires estimates of the uncertainties in the meteor velocity and direction. A single-body or a gross-fragmentation solution gives these estimates directly.

There may be more than one single-body or gross-fragmentation solution to a meteor. Each photograph of the meteor gives one solution. Assume that we have two single-body solutions of a meteor, one for each photograph. Denote the values for each solution x_1 and x_2 (where x is the speed at first measured point or the cross-section to mass ratio of the meteoroid), with their associated "inner" errors σ_1 and σ_2. We now estimate the "outer" error, σ, accounting for both solutions (Ceplecha, private communication). If the "inner" error of one solution is larger than three times that of the other solution, it is discarded from further analysis. The weighted mean of x is computed as

$$x = \frac{x_1/\sigma_1^2 + x_2/\sigma_2^2}{1/\sigma_1^2 + 1/\sigma_2^2},$$

and the "outer" error is

$$\sigma = \sqrt{\frac{(x-x_1)^2/\sigma_1^2 + (x-x_2)^2/\sigma_2^2}{1/\sigma_1^2 + 1/\sigma_2^2}}.$$

We consider two different meteoroid streams, the Geminids and the Taurids. The Geminid meteoroid stream is thought to be young and narrow since the meteors are observed

only during a few days. On the other hand, the Taurid meteoroid stream is thought to be old and dispersed since it is observed over several months. Both meteoroid streams have proposed parent bodies; asteroid 3200 Phaethon and comet P/Encke, respectively.

The meteors are taken from three different observing programs; the Harvard Small Camera Program (hereafter HSC) operated during 1936-1952, the Harvard Super-Schmidt (HSS) Program (1952-1959), and the Prairie Network (PN) Fireball Program (1963-1975). Both the HSC program and the HSS program detected faint, small meteoroids ($\approx$ 1 g), while the PN program photographed massive ($\approx$ 1 kg), potentially meteorite dropping fireballs.

Harvard Small Camera Program

Harvard small camera double station meteors were photographed from the Cambridge and Oak Ridge (later Agassiz) stations of the Harvard Observatory, Massachusetts, in the period 1936-1952. The stations were moved to Doña Ana and Soledad Canyon, New Mexico, in 1952. Table 5-1 (Jacchia, 1952) gives the station coordinates. The baseline between the Massachusetts stations is 37.896 km long; the baseline in New Mexico is 28.567 km.

5-1 Massachusetts and New Mexico HSC stations

Station	Oak Ridge (Agassiz)	Cambridge
Longitude (W), λ	71°33'29".82	71°7'45".45
Latitude (N), ϕ	42°30'20".72	42°22'53".70
H (m)	190.2	18.3
Station	Doña Ana	Soledad Canyon
Longitude (W), λ	106°47'58".50	106°36'42".32
Latitude (N), ϕ	32°30'21".94	32°18'13".61
H (m)	1412.3	1567.4

Table 5-2 (Jacchia, 1952) gives data on the cameras and the shutters. The quantity r.p.m. is the number of revolutions per minute of the rotating shutter associated with the camera, and n is the number of measurable features (breaks and/or dots) per shutter revolution. The timing of the meteor event was not accurately known at the Massachusetts stations; visual timing was used at the New Mexico stations. However, when flares in the meteor trail, bright enough to trigger a photodetector, can be identified and measured from both stations, the instant of the meteor can be determined independently from each flare (Whipple & Jacchia, 1957).

Table 5-2 HSC Meteor Cameras at Massachusetts and New Mexico

Station	Camera	Aperture (inches)	f (inches)	r.p.m.	n
Oak Ridge	AI	1.5	6	600	2
Cambridge	FA	1.5	6	600	2
Doña Ana	AI	1.5	6	740	4
Soledad	FA	1.5	6	630	4

George Wetherill (Carnegie Institute) provided us with original meteor data for 69 HSC meteors. Each meteor is documented on large, hand written paper sheets. These data contain all computations made to reach the dynamic and photometric meteor quantities. Out of the 69 meteors we initially selected all Geminid meteors; 59 all together.

The pre-atmospheric velocity, v_∞, was computed according to the traditional interpolation polynomial (Whipple, 1938; Whipple & Jacchia, 1957). As pointed out in chapter 3, we would rather use a single-body or a gross-fragmentation solution, than the non-physical

interpolation polynomial. Ceplecha (Ondřejov Observatory) provided us with the single-body and gross-fragmentation code, written in FORTRAN.

Ceplecha's code requires time, t_i, distance along the trail, l_i, and height, h_i, in the atmosphere, where i denotes a measured point on the meteor trail. Time and distance along the trail are given explicitly on the hand written sheets. Determining the height in the Earth's atmosphere is a more complicated matter.

We now describe how to get the height in the atmosphere from the hand written sheets. Equation (28) in Whipple and Jacchia (1957)

$$H_i = h_{Ai} + H_A + \delta h_{Ai},$$

where the subscript A denotes observing station A, H_i is the height above sea level, H_A elevation of station above sea level, and δh_{Ai} is a correction for the curvature of the geoid. The quantity h_{Ai} is the height above the plane normal to the zenith direction (at station A) computed as

$$h_{Ai} = C_1 - \cos z_{Ar} l,$$

where C_1 is the height in the atmosphere when $l = 0$, and z_{Ar} is the zenith distance of the meteor radiant with respect to station A, and the entries in this equation are given explicitly on the hand written sheets.

The quantity δh_{Ai} is interpolated from a few (five to ten) heights where δh_{Ai} is explicitly given as a function of h_{Ai}. The height in the atmosphere, h_i, is computed as

$$h_i = h_{Ai} + \delta h_{Ai}.$$

The HSC meteors are not corrected for gravity. The spatial deflection of a meteoroid

from its purely inertial trajectory, due to gravity, at a given point i is

$$G_i = \frac{1}{2}\frac{GM_E}{(R_E+h_i)^2}t_i^2,$$

where t_i is the time elapsed from the instant of the first break. The distances along the trail are corrected as

$$l_{i,corr} = l_i - G_i \cos z_R,$$

and the height in the atmosphere is corrected as

$$h_{i,corr} = h_i + G_i.$$

We are now ready to feed Ceplecha's code with t_i, $l_{i,corr}$, and $h_{i,corr}$.

Out of the 59 HSC Geminid meteors, 17 have been successfully interpreted through the single-body code. We do not use the gross-fragmentation code for the small camera Geminids. Table 5-3 gives the meteor number, the year, the date, the observing station, and the number of breaks, n_b, on the meteor trail for the HSC Geminid photographs yielding a single-body solution. In addition to this, table 5-3 also gives the zenith distance and the estimated mass (through integration of the meteor radiation, called photometric mass, see Bronshten, 1983, for a review) of the meteoroid.

Table 5-3 HSC Geminids: Basic data

No.	Year	Date	Station	n_b	$\cos z_R$	m (g)
1112	1941	Dec 11.266377	Oak Ridge	18	0.984	6.0
1265	1944	Dec 11.218003	Oak Ridge	13	0.933	9.7
1639	1947	Dec 14.239583	Oak Ridge	26	0.898	140
2283	1950	Dec 11.135417	Doña Ana	24	0.349	0.2
2290	1950	Dec 12.127662	Soledad	57	0.312	18
2298	1950	Dec 12.222417	Soledad	26	0.804	1.2
2357	1950	Dec 14.240236	Soledad	37	0.931	83
2357	1950	Dec 14.240236	Doña Ana	57	0.931	83
2377	1950	Dec 14.385353	Soledad	36	1.000	1.8
2385	1950	Dec 14.341472	Doña Ana	17	0.972	0.5
2390	1950	Dec 14.332407	Doña Ana	27	0.972	2.3
2390	1950	Dec 14.318380	Doña Ana	37	0.946	9.7
2501	1950	Dec 13.282700	Doña Ana	26	0.867	0.1
2537	1950	Dec 14.324780	Doña Ana	80	0.953	0.5
2537	1950	Dec 15.260417	Soledad	18	0.804	0.1
2538	1950	Dec 13.176944	Doña Ana	73	0.505	0.5
2588	1950	Dec 14.332338	Doña Ana	44	0.965	0.2
2591	1950	Dec 14.290313	Doña Ana	37	0.889	0.1

Table 5-4 gives the input data for the Parent-Daughter association method. The single-body code is used on the meteor data to find the input data; the speed of the meteoroid at first measured point and the cross-section to mass ratio (where we assume $C_D = 2$, see chapter 4), with associated uncertainty estimates. The estimate of the uncertainty in the radiant, $\sigma_r = 0.02$ degrees, is adopted from Whipple (1947), and is not an output from the single-body code. The latitude and longitude of the first measured point is estimated as the average latitude and longitude of the two observing stations; $\lambda = 71°20'20".41$ and $\phi = 42°26'37".21$ in

Massachusetts, λ = 106°42'20".41 and ϕ = 32°24'17".78 in New Mexico.

5-4 Single-body solution data for HSC Geminids

No.	$v_0 \pm \sigma(v_0)$ (km/sec)	h_0 (km)	α (deg)	δ (deg)	σ_r (deg)	$A/m \pm \sigma(A/m)$ (cm^2/g)
1112	37.33±0.09	78.95	110.75	33.25	0.02	0.19±0.05
1265	36.30±0.03	85.65	110.01	32.26	0.02	0.40±0.04
1539	36.37±0.02	96.37	113.16	32.81	0.02	0.136±0.005
2283	36.08±0.09	93.70	107.55	32.88	0.02	3.6±0.9
2290	35.95±0.01	99.28	108.95	33.11	0.02	0.46±0.08
2298	35.29±0.09	90.03	109.41	31.23	0.02	1.73±0.34
2357	35.85±0.02	91.19	113.14	32.71	0.02	0.275±0.002
2377	36.31±0.02	95.62	113.78	32.37	0.02	0.89±0.15
2385	36.21±0.05	93.41	113.97	32.20	0.02	1.21±0.31
2390	36.14±0.02	88.97	113.36	32.26	0.02	0.73±0.05
2394	35.94±0.02	96.71	113.25	32.80	0.02	0.88±0.06
2501	35.91±0.10	91.87	111.72	32.56	0.02	1.04±0.55
2537	36.28±0.02	90.56	113.31	32.32	0.02	0.96±0.02
2547	36.8±1.2	87.76	113.08	31.78	0.02	5.5±2.5
2548	39.95±0.01	98.29	110.29	32.88	0.02	1.34±0.03
2588	35.98±0.06	90.25	113.42	31.92	0.02	1.32±0.24
2591	36.46±0.10	95.93	112.68	32.39	0.02	1.9±1.0

The Harvard Super-Schmidt program (Jacchia & Whipple, 1956) gave some 6,000 doubly photographed meteors. The HSS stations were located in New Mexico; Doña Ana and Soledad from March 1952-June 1954, and Sacramento Peak and Mayhill from July 1954-1959.

The Baker Super-Schmidt cameras - with an aperture of twelve inches, a focal length of eight inches, and an overall optical design optimized for meteor photography - increased the observation rate with a factor of ≈ 1,000, compared to the patrol cameras used in the HSC program. The shutter, with two 45° degree openings rotating at 1,800 r.p.m., interrupted the meteor trail 60 times a second. The timing of the meteor was made visually, and the error is estimated as ±2 seconds.

The 413 longest and brightest trails, from the 3,500 doubly photographed meteors at Doña Ana and Soledad, were selected by Jacchia and Whipple (1961), to compute their heliocentric orbits and. Due to the selection, the sample is not random among the observed meteors. Later, Jacchia et al. (1967) analyzed the physical aspect of the atmospheric entry for the same sample. These 413 meteors comprise the most accurate and precise orbital and atmospheric data of photographic meteors. The data consists of 290 sporadic and 123 stream meteoroids (based on orbital similarities).

The 413 meteors have not been analyzed with Ceplecha's single-body code. Unfortunately, the original, hand written meteor data is not readily available at the Smithsonian Astrophysical Observatory. However, Ceplecha (private communication), while visiting the Smithsonian Astrophysical Observatory, successfully applied his single-body code to a few Geminids, and he found the solution to be within the error estimates of Jacchia et al. (1967).

With this in mind, we assume that the meteors in Jacchia et al. (1967) behave according to the single-body theory.

Jacchia et al. (1967) provide dynamic data at a few points for most of the 413 meteors (tables 1.1 and 1.2 in their paper). We now describe a new method of how to estimate the input data for the Parent-Daughter association method. It has to be pointed out though, that the data used is not the raw data from meteor photographs, but based on the interpolation polynomial.

The data we use from table 1.1 (Jacchia et al., 1967) is; the pre-atmospheric speed, v_∞, the ablation coefficient, σ, the zenith distance, $\cos z_R$, the height in the atmosphere at first measured point, h_0. From table 1.2 we take the deceleration, $\dot{v}$, with probable error, $\sigma(\dot{v})$, the speed, v, and the height, h, for the two points with greatest height in the atmosphere. The idea here, is to use the error in the deceleration, and propagate it to error estimates of v_∞, σ, and $(C_D/2)(A/m)$.

We find the error estimates of v_∞ and σ by using single-body theory (Pecina & Ceplecha, 1983, which we have extended to account for a non-isothermal atmosphere)

$$\dot{v}_i = \frac{1}{2}\frac{\rho(h_i)}{\int_{h_i}^{\infty}\rho\, dh}\cos z_R v_i^2 \exp(-\frac{\sigma}{6}v_i^2)[Ei(\frac{\sigma}{6}v_\infty^2) - Ei(\frac{\sigma}{6}v_i^2)],$$

where i = 1 or 2 denoting the two points in the atmosphere, the air density ρ is taken from CIRA 72 monthly atmosphere, and $Ei(x) = \int_{-\infty}^{x}(\exp(t)/t)dt$ is the exponential integral. We sample the deceleration at both heights 100 times from its probable error distribution, which is assumed to be Gaussian. For each of these samples we solve the preceding two equations (one for each point i in the atmosphere) for v_∞ and σ by an iterative two-dimensional Newton-Raphson scheme (Press et al, 1992). Effectively we force the meteor to behave according to single-body theory. However, not all samples of the decelerations yield a solution.

Assume that n_s of the 100 samples are successful, yielding $v_{\infty j}$ and σ_j ($j = 1, ..., n_s$). We then compute, using the deceleration equation and the mass-loss equation,

$$(\frac{C_D}{2}\frac{A}{m})_j = \frac{-\dot{v}_{1,j}}{\rho(h_1)v_1^2 \exp[\sigma_j/6(v_{\infty j}^2 - v_1^2)]},$$

yielding n_s values of $(C_D/2)(A/m)$. To estimate the speed at first measured point, we integrate the differential equation (found through the use of the three basic equations of the single-body theory; the deceleration equation, the mass-loss equation, and the height equation):

$$\frac{dv}{dh} = (\frac{C_D}{2}\frac{A}{m})_j \frac{\rho v^2}{\cos z_R} \exp[\frac{\sigma_j}{6}(v_{\infty j}^2 - v^2)],$$

from height h_1 to h_0, for $j = 1,...,n_s$.

We have finally reached the input for the Parent-Daughter association method. The mean and the "inner" errors of the input quantities, v_0 and $(C_D/2)(A/m)$, are computed as

$$x = \frac{1}{n_s}\sum_{j=1}^{n_s} x_j$$

$$\sigma(x) = \sqrt{\frac{\sum_{j=1}^{n_s}(x - x_j)^2}{n_s - 1}},$$

where x is v_0 or $(C_D/2)(A/m)$. The errors above are "inner" errors. If more than one solution exists, we compute the weighted mean and the "outer" error as discussed in the beginning of the chapter.

There are 20 Geminids and 24 Taurids (18 Southern Taurids, with questionable members included, and six Northern Taurids) in Jacchia et al. (1967). Five Geminids (meteor

numbers: 5605, 8645, 9418, 9725, and 9749) have a solution according to the method described above. Three of these Geminids (5605, 9725, and 9749) have two solutions. The remaining 15 Geminids have the deceleration given at only one height per observing station. This is not enough data, since the method requires deceleration at two points. Fourteen Southern Taurids have solutions. Seven (2961 (photographed in 1951 at Soledad, before the HSS program was completely operative), 4507, 4701, 5022, 8945, 9104, and 9238) have one solution, and seven (3886, 5176, 5195, 5346, 8990, 9015, and 9416) have two solutions. Four Northern Taurids (5257, 5511, 9257, and 9331) have one solution, and none have two solutions. The remaining six Taurids have deceleration given at only one height in the atmosphere.

The data on the HSS Geminids are given in tables 5-5 and 5-6, and the data on the HSS Taurids are presented in tables 5-7 and 5-8. The zenith distances and the mass estimates ($m_{\infty 2}$ in table 1.1) are from Jacchia et al. (1967). The error in the radiant, σ_r, is estimated from the quality class of the meteor (Jacchia & Whipple, 1961).

The Geminid average "outer" error is 0.08% for v_0 and 2.0% for A/m (where $C_D = 2$ is assumed). The corresponding Taurid "outer" errors are 0.1% and 10% respectively. If the "inner" error is larger than the "outer" error for a meteor with only one solution, we use the "inner" error.

Table 5-5 HSS Geminids: Basic data

No.	Year	Date	$\cos z_R$	mass(g)
5605	1952	Dec. 11.21585	0.658	3.3
8645	1953	Dec. 13.34920	0.984	4.4
9418	1953	Dec. 7.40209	0.993	0.4
9725	1953	Dec. 14.37895	1.000	2.8
9749	1953	Dec. 14.40912	0.991	1.6

Table 5-6 Solutions for HSS Geminids

No.	$v_0 \pm \sigma(v_0)$ (km/sec)	h_0 (km)	α (deg)	δ (deg)	σ_r (deg)	$A/m \pm \sigma(A/m)$ (cm^2/g)
5605	36.19±0.03	101.3	109.52	32.73	0.01	01.52±0.04
8645	36.24±0.03	102.2	112.77	32.35	0.01	0.94±0.02
9418	36.24±0.03	98.1	105.95	32.10	0.01	3.2±0.4
9725	36.07±0.04	92.2	114.20	32.52	0.01	1.06±0.04
9749	36.21±0.01	100.3	114.10	32.38	0.01	0.8±0.2

Table 5-7 HSS Taurids: Basic data

No.	Year	Date	$\cos z_R$	mass (g)
2961	1951	Oct. 2.22043	0.790	0.37
3886	1952	Sep. 1.47897	0.589	0.05
4507	1952	Sep. 20.38472	0.820	0.01
4701	1952	Sep. 30.48305	0.589	0.02
5022	1952	Oct. 21.40054	0.589	0.13
5176	1952	Oct. 23.42865	0.795	0.11
5195	1952	Oct. 23.48194	0.572	0.05

Table 5-7 -- continued

No.	Year	Date	$\cos z_R$	mass (g)
5257	1952	Oct. 24.38896	0.924	0.16
5346	1952	Nov. 11.21208	0.790	0.03
5511	1952	Nov 21.44139	0.750	0.07
8945	1953	Oct. 9.19547	0.615	0.01
8990	1953	Oct. 9.47638	0.713	0.02
9015	1953	Oct. 10.29028	0.878	0.07
9104	1953	Oct. 20.47562	0.651	0.07
9238	1953	Nov. 7.37403	0.906	0.03
9257	1953	Nov.7.48135	0.632	0.27
9331	1953	Nov.13.35062	0.978	0.26
9416	1953	Dec. 7.39528	0.841	0.12

Table 5-8 Solutions for HSS Taurids

No.	$v_0 \pm \sigma(v_0)$ (km/sec)	h_0 (km)	α (deg)	δ (deg)	σ_r (deg)	$A/m \pm \sigma(A/m)$ (cm^2/g)
2961	31.12±0.03	94.4	15.85	10.20	0.02	2.7±0.5
3886	29.10±0.04	101.5	-3.70	0.58	0.01	6.4±0.1
4507	29.98±0.03	99.5	16.67	0.25	0.06	4.9±1.4
4701	29.98±0.03	99.7	25.73	5.83	0.02	5.8±0.6
5022	30.09±0.03	100.5	41.23	11.20	0.01	4.8±0.6
5176	30.44±0.05	102.3	44.07	12.50	0.01	4.6±0.2
5195	28.87±0.01	102.1	42.38	12.05	0.01	7.6±0.4
5257	32.87±0.03	102.0	45.28	19.58	0.01	1.4±0.2
5346	28.75±0.02	102.3	56.83	15.07	0.01	6.3±1.0
5511	30.99±0.03	104.9	67.05	21.93	0.01	4.8±0.5

Table 5-8 -- continued

No.	$v_0 \pm \sigma(v_0)$ (km/sec)	h_0 (km)	α (deg)	δ (deg)	σ_r (deg)	$A/m \pm \sigma(A/m)$ (cm^2/g)
8945	30.99±0.03	102.2	32.62	9.87	0.01	6.1±0.7
8990	26.93±0.05	100.2	39.02	12.22	0.01	6.3±1.6
9015	30.88±0.04	103.5	32.62	8.23	0.01	1.6±0.2
9104	30.18±0.03	100.9	43.67	12.17	0.01	5.7±0.6
9238	28.22±0.03	100.6	55.28	14.17	0.01	5.0±1.0
9257	30.35±0.03	103.7	55.97	22.43	0.01	3.4±0.3
9331	30.80±0.03	105.3	62.23	23.77	0.01	3.0±0.3
9416	25.61±0.01	100.2	80.02	16.00	0.01	4.1±01

Prairie Network

During 1963-1975, the Smithsonian Astrophysical Observatory operated the Prairie Network (PN). The program consisted of 16 stations in the Midwestern USA (McCrosky & Boeschenstein, 1965), and it was aimed for recording, photographically, bright (fireballs), long duration ($t > 1$ second) meteors, since the chance of finding a belonging meteorite is increased. However, only one meteorite was recovered; Lost City (McCrosky et al., 1971). The baseline between PN stations is approximately 300 km, a factor ten times larger than that of the Harvard programs. Because of the long baseline, the cameras were aimed at the horizon.

More than 2,700 fireballs were recorded, but less than 1,000 have been reduced. The reduction accounts for atmospheric refraction, departure from a linear meteor trail due to gravity, and for imperfections in the optical system (McCrosky & Posen, 1968). The optical system had an aperture of ten inches and a focal length of eight inches. Only the brightest

meteors (fireballs) could be recorded. The visual meteors photographed under the Harvard programs, would not have been recorded under the PN program. A coded switching shutter, operated by relays, gives an accuracy of ± 10 seconds in the timing of the meteor.

The PN was biased in favor "asteroidal" fireballs, since they are thought to be made of tougher material, implying a greater chance of producing meteorites. However, a few meteoroid stream fireballs (thought to be made of fragile "cometary" material) were recorded. To extend the data base of observed Geminids, McCrosky (unpublished) reduced 56 PN Geminids. Ceplecha (private communication) has provided us with single-body meteor solutions for 43 of the 56 PN Geminids. Of the remaining 13 PN Geminids, eleven have no single-body solution, and two were obviously wrongly classified as Geminids (atmospheric impact speeds of 14 and 22 km sec^{-1}). In addition to the PN Geminids, Ceplecha also provided us with eight PN Taurids; four Southern Taurids (PN numbers: 39093, 39418, 39424, and 39424) and four Northern Taurids (39085, 39424, 39775, and 39833). Two of the Taurids have gross-fragmentation solutions; 39424, and 39775.

Twelve of the PN Geminids have two single-body solutions. The "outer" errors are on average 0.2% in v_0, and 17% in A/m. These "outer" errors are applied to the remaining 31 PN Geminids.

The error associated with the radiant is estimated (Ceplecha, private communication) as

$$\sigma_r = \arctan\left(\frac{2\sigma_l}{L}\right),$$

where L is the total length of the trajectory and σ_l is the error in distance along the trajectory for one measured point. It is implicitly assumed that the geometrical precision perpendicular to the trajectory is the same as along the trajectory. When this is applied to the twelve PN

Geminids with two single-body solutions, it is found that the average "outer" error amounts to $\sigma_r = 0.12$ degrees, and is used on the remaining PN Geminids.

All errors for the eight PN Taurids are "inner" errors. This is since only one single-body or gross-fragmentation solution was found for each Taurid, and no estimate of the "outer" errors is therefore possible.

Tables 5-9 and 5-10 gives the data for the PN Geminids. The twelve PN Geminids with two single-body solutions are given first. The first column, denoted G. No., refers to the number McCrosky originally assigned to each PN Geminid photography. The photometric mass estimates conform with Ceplecha (1988).

Tables 5-11 and 5-12 provides the data on the eight PN Taurids. The Taurids are given in increasing PN number. The mass estimate is dynamical, not photometric (see Bronshten, 1983, for review on how to reconcile the two mass-scales).

Table 5-9 PN Geminids: Basic data

G. No.	Year	Date	h_0(km)	$\cos z_R$	mass (kg)
001,003	1966	Dec. 14.3241	83.3	0.957	1.1
013,030	1968	Dec. 14.1414	90.0	0.503	2.0
018,020	1968	Dec. 14.4789	92.3	0.834	0.68
023,024	1968	Dec. 14.3788	85.2	0.978	0.19
027,028	1968	Dec. 14.3641	84.3	0.992	0.38
064,065	1968	Dec. 14.1956	89.0	0.672	0.09
067,068	1968	Dec. 14.1805	94.3	0.621	0.09
081,082	1969	Dec. 14.4260	85.7	0.962	0.04
085,086	1969	Dec. 14.3255	82.1	0.991	-
105,106	1968	Dec. 13.2884	84.2	0.910	1.3

Table 5-9 -- continued

G. No.	Year	Date	h_0(km)	$\cos z_R$	mass (kg)
110,119	1966	Dec. 14.3355	83.2	0.932	0.35
118,119	1966	Dec. 13.1966	79.5	0.732	0.05
009	1966	Dec. 14.2482	94.7	0.866	2.0
009	1966	Dec. 14.2591	85.4	0.885	0.09
012	1968	Dec. 14.1212	87.7	0.407	0.05
022	1968	Dec. 14.4113	83.2	0.932	-
025	1970	Dec. 14.2991	83.2	0.968	0.03
031	1968	Dec. 14.2764	90.5	0.914	0.03
039	1968	Dec. 13.3299	92.0	0.986	1.2
039	1968	Dec. 12.1855	85.6	0.664	0.43
041	1968	Dec. 14.2377	83.1	0.868	0.43
044	1968	Dec. 13.3299	91.0	0.991	0.43
050	1968	Dec. 12.3670	83.1	0.983	0.06
051	1968	Dec. 14.2847	88.8	0.932	0.03
057	1968	Dec. 12.2409	88.8	0.832	0.06
060	1968	Dec. 11.2935	91.4	0.986	0.01
069	1968	Dec. 14.1449	90.5	0.481	0.05
073	1968	Dec. 14.1665	86.1	0.591	0.06
076	1969	Dec. 14.5232	90.8	0.711	-
079	1969	Dec. 14.3438	85.8	0.997	0.07
083	1969	Dec. 14.3355	91.0	0.997	0.07
087	1969	Dec. 14.2194	79.5	0.747	0.05
089	1969	Dec. 14.2128	85.8	0.745	0.03
092	1969	Dec. 14.1333	91.9	0.492	0.08
093	1969	Dec. 14.4383	97.9	0.923	0.04
095	1969	Dec. 14.1941	89.5	0.993	0.46

Table 5-9 -- continued

G. No.	Year	Date	h_0(km)	$\cos z_R$	mass (kg)
099	1969	Dec. 14.3385	94.1	0.992	0.06
102	1969	Dec. 14.2919	87.4	0.936	0.12
103	1969	Dec. 14.3286	90.8	0.992	0.04
102	1966	Dec. 14.3841	86.5	0.978	0.08
115	1966	Dec. 14.2927	75.1	0.956	0.08
124	1967	Dec. 13.4061	82.8	0.980	0.39
127	1966	Dec. 14.1941	88.7	0.691	0.09

Table 5-10 Single-body solutions for PN Geminids

G. No.	$v_0 \pm \sigma(v_0)$ (km/sec)	α (deg)	δ (deg)	σ_r (deg)	$A/m \pm \sigma(A/m)$ (cm^2/g)
001,003	35.81±0.03	113.55	32.61	0.08	0.101±0.007
013,030	35.79±0.12	112.38	32.94	0.06	0.032±0.012
018,020	34.79±0.08	115.04	32.61	0.08	0.10±0.01
023,024	36.18±0.03	115.47	32.80	0.13	0.24±0.13
027,028	36.21±0.26	114.72	32.41	0.10	0.19±0.03
064,065	36.08±0.07	112.78	32.48	0.16	0.29±0.05
067,068	35.65±0.01	112.77	32.32	0.10	0.24±0.01
081,082	36.05±0.23	116.22	34.46	0.16	0.399±0.004
085,086	34.95±0.04	113.88	31.95	0.10	0.122±0.004
105,106	35.64±0.07	113.88	31.77	0.26	0.140±0.007
110,111	36.03±0.14	114.22	32.83	0.16	0.10±0.06
118,119	35.57±0.05	111.60	33.14	0.10	0.077±0.005
006	35.51±0.08	111.69	33.33	0.12	0.18±0.03
009	35.42±0.07	112.38	32.52	0.12	0.13±0.02

Table 5-10 -- continued

G. No.	$v_0 \pm \sigma(v_0)$ (km/sec)	α (deg)	δ (deg)	σ_r (deg)	$A/m \pm \sigma(A/m)$ (cm^2/g)
092	35.75±0.07	111.98	32.88	0.12	0.30±0.05
022	36.07±0.07	114.53	32.09	0.12	0.34±0.06
025	35.44±0.07	114.53	33.23	0.12	0.17±0.03
031	35.51±0.07	115.23	32.53	0.12	0.31±0.05
031	36.66±0.07	113.90	32.34	0.12	0.09±0.01
039	37.38±0.08	109.80	31.72	0.12	0.13±0.02
041	35.75±0.07	113.42	32.70	0.12	0.11±0.02
044	35.85±0.07	113.90	32.47	0.12	0.10±0.02
089	36.07±0.07	112.44	32.08	0.12	0.17±0.03
051	36.58±0.07	113.90	32.36	0.12	0.63±0.11
089	35.44±0.07	110.11	32.70	0.12	0.22±0.04
060	34.30±0.07	107.24	33.13	0.12	0.28±0.05
069	36.31±0.07	112.19	31.98	0.12	0.44±0.08
073	36.66±0.07	112.28	32.30	0.12	0.81±0.14
079	35.39±0.07	115.86	32.88	0.12	0.19±0.03
079	35.39±0.07	111.75	32.51	0.12	0.19±0.03
073	35.85±0.07	113.90	32.34	0.12	0.19±0.03
089	35.77±0.08	113.26	32.34	0.12	0.13±0.03
089	35.85±0.07	112.19	32.36	0.12	0.50±0.08
092	36.32±0.07	113.43	33.09	0.12	0.21±0.04
093	35.33±0.07	114.77	32.34	0.12	0.28±0.05
095	35.33±0.07	113.41	32.29	0.12	0.09±0.02
099	35.87±0.07	114.41	32.17	0.12	0.20±0.03
102	36.48±0.07	113.30	32.11	0.12	0.27±0.05
103	35.93±0.07	114.40	31.79	0.12	0.26±0.04

Table 5-10 -- continued

G. No.	$v_0 \pm \sigma(v_0)$ (km/sec)	α (deg)	δ (deg)	σ_r (deg)	$A/m \pm \sigma(A/m)$ (cm^2/g)
112	35.67±0.07	114.60	32.85	0.12	0.21±0.04
115	36.28±0.07	113.44	33.05	0.12	0.11±0.02
124	34.91±0.07	115.44	34.00	0.12	0.17±0.03
127	36.45±0.07	111.95	32.34	0.12	0.39±0.07

Table 5-11 PN Taurids: Basic data

PN No.	Year	Date	h_0(km)	$\cos z_R$	mass (kg)
39085	1965	Nov. 21.4706	96.4	0.891	0.03
39093	1965	Nov. 29.4769	79.5	0.485	0.11
39418	1966	Oct. 20.2126	84.5	0.650	0.05
39423	1966	Oct. 25.2232	83.7	0.891	0.10
39424	1966	Oct. 26.4659	80.6	0.394	0.34
39460	1966	Dec. 1.0994	81.5	0.490	0.02
39775	1967	Oct. 12.2782	78.8	0.903	0.67
39833	1967	Dec. 9.0298	97.8	0.280	0.01

Table 5-12 Solutions to PN Taurids

PN No.	$v_0 \pm \sigma(v_0)$ (km/sec)	α (deg)	δ (deg)	σ_r (deg)	$A/m \pm \sigma(A/m)$ (cm^2/g)
39085	28.50±0.01	65.60	25.49	0.06	0.250±0.009
39093	29.17±0.02	77.14	19.15	0.07	0.143±0.005
39418	29.88±0.01	36.79	-1.30	0.06	0.136±0.002
39423	34.19±0.04	44.81	24.18	0.08	0.110±0.010
39424	26.68±0.01	37.49	8.38	0.02	0.072±0.003

Table 5-12 -- continued

PN No.	$v_0 \pm \sigma(v_0)$ (km/sec)	α (deg)	δ (deg)	σ_r (deg)	$A/m \pm \sigma(A/m)$ (cm^2/g)
39460	30.55±0.02	76.74	18.53	0.06	0.174±0.002
39755	26.19±0.01	22.59	13.16	0.03	0.053±0.001
39833	30.31±0.01	82.36	28.09	0.03	0.325±0.009

Parent Bodies

Geminids: 3200 Phaethon, 1566 Icarus, 5786 Talos

In October 1983, S. Green reported (IAU circular No. 3878) the discovery of a fast-moving object, 1983 TB, in the data gathered by the Infrared Astronomical Satellite (IRAS). A few days later, F. L. Whipple (IAU circular 3881) pointed out that the orbit coincide with those of Geminid meteoroids. The fast-moving object was classified as an Apollo asteroid, and named 3200 Phaethon.

Green et al. (1985) presented infrared observations from 1-20 μm, and interpreted them as being due to an asteroid, 4.7±0.5 km in diameter. The asteroid was further classified as B class, having a surface with the thermal properties of solid rock. Observations (Cochran & Barker, 1984) show no cometary emission from Phaethon at 1.7 AU. This, however, does not rule out a cometary origin, merely indicating that the object was not active at the time. D. J. Tholen (IAU circular No. 4034) reported a rotation period slightly less than four hours.

Table 5-13 Orbital elements of proposed Geminid parent bodies

Parent Body	3200 Phaethon	1566 Icarus	5786 Talos
a (AU)	1.2713207	1.0780404	1.0815194
e	0.8901151	0.8267397	0.8268023
i (deg)	22.09121	22.88162	23.24577
Ω (deg)	265.61146	88.15857	161.37402
ω (deg)	321.79290	31.22221	8.26850
T	920407.15792	921214.91154	930723.60679
Epoch	930113.0	930113.0	940217.0
MPC	19988	8665	940217

To search for other possible parent bodies of the Geminid meteoroid stream, we searched the Near Earth Asteroid (NEA) data disseminated through an email service of Duncan Steel (Anglo-Australian Observatory). The two objects with closest orbital similarities ($D' < 0.15$) are 1566 Icarus and 5786 Talos. Table 5-13 provides the orbital elements (in J2000.0) of the proposed parent bodies; semi-major axis a, eccentricity e, inclination i, longitude of ascending node Ω, argument of perihelion ω, and time of perihelion passage T, for a specific epoch. The data is taken from Minor Planet Circulars (MPC).

Taurids: P/Encke

Short-period comet P/Encke, named after J. F. Encke who was the first to calculate its orbit, has the shortest orbital period of any known comet; only 3.3 years. Since its discovery in 1786, it has made 64 revolutions around the Sun. It is likely that the nucleus, with an estimated diameter of 4.4-9.8 km (Luu & Jewitt, 1990), is only the remaining central part of an originally much larger body.

It was soon realized by J. F. Encke that the comet is subject to non-gravitational forces; it persisted to arrive 2.5 hours too early every return. Encke proposed a "thin etherial medium" that resists the motion of an extremely tenuous comet, but does not affect the motions of the massive planets. The acceleration, among other cometary phenomena, of comets in general, and for comet P/Encke in particular, was explained by Whipple (1950b). We now understand that the motion of P/Encke is dependent on several parameters (Whipple & Sekanina, 1979); e.g., the shape, the orientation and precession of the spin axis, and the spin period (≈ 6.5 hours). The orbital elements (in J2000.0) for P/Encke are given in table 5-14.

Table 5-14 Orbital elements of comet P/Encke

Parent Body	P/Encke
a (AU)	2.2095052
e	0.8500146
i (deg)	11.92974
Ω (deg)	334.72236
ω (deg)	186.27131
T	970523.59506
Epoch	970601.0
MPC	23483

Computations and Hardware

All integrations have been made using the 15-th order RADAU integrator by Everhart (1985). The subroutine, RA15, is written in FORTRAN. Carusi et al. (1985) found the integrator to provide one of the best accuracy/speed ratios for barycentric equations of motion.

The computations are made on an IBM/6000-350 and an IBM/6000-220. The IBM/6000-350 is slightly more than twice as fast as the IBM/6000-220. A FORTRAN pre-compiler is available for IBM/6000 machines, and it increases the speed of the computations by nearly a factor two on both machines.

Integration of 50 sampled Geminid orbits, 7,000 years back in time, requires ≈ 38 hours of CPU time on the IBM/6000-350, and 5.4 MByte of disk space.

CHAPTER 6
CROSS-SECTION TO MASS RATIO

This chapter discuss implications of the cross-section to mass ratio parameter. It is customary in meteor physics to treat meteoroids as spherical in shape. The reason for this approach is that the mathematical formulation of the problem is simple. However, a spherical shape is extreme, and may only serve as a first approximation. A non-spherical treatment is more difficult, since we do not only have to take the shape of the meteoroid into account, but also the spin state (spin axis orientation and spin period) of the meteoroid.

The cross-section to mass ratio, A/m, the estimated photometric mass, m_{ph}, and an assumption of the shape of a meteoroid allows an estimate for the bulk density ρ_{bulk}. We may write (where $C_D = 2$ is assumed)

$$\rho_{bulk} = [F/(A/m)]^{3/2} m_{ph}^{-1/2},$$

where $F = A/V^{2/3}$ is the shape factor and V is the volume of the meteoroid. Note that the uncertainty of the estimated bulk density depends more on the shape factor and the cross-section of the meteoroid, than on the mass estimate.

An assumption of the shape is vital to the estimated bulk density. The shape factor of a sphere is 1.21, and 0.44 and 1.92 for a cylinder flying flat end first with a ratio of diameter to length of 1/3 and 3, respectively. The values for the cylinder case corresponds to a factor of 9 in bulk density. From this it is seen that a poorly constrained shape factor can generate almost any value of the bulk density. Further, from the above equation it is seen that a

meteoroid presenting its smallest cross-section yields an apparent high bulk density when interpreted as being spherical in shape, and, conversely, a meteoroid presenting its largest cross-section to mass ratio yields an apparent low bulk density.

Figure 6-1 shows the pre-atmospheric mass ratio of Geminids as a function of their estimated photometric mass. The filled triangles, circles, and squares correspond to HSC (17 from chapter 5), HSS (five from chapter 5), and PN (40 with mass estimates from chapter 5) Geminids, respectively. The open circles correspond to values of A/m, based on the interpolation polynomials, taken from Gustafson and Adolfsson (1996). The dotted, dashed, and solid lines correspond to a sphere of density 0.25, 1.0, and 2.54 g cm^{-3}, respectively. Figure 6-2 shows the same as in Figure 6-1, but for the Taurids presented in chapter 5. All symbols have the same meaning as in Figure 6-1.

On average, it appears that the Geminids have a bulk density of 1 g cm^{-3}. However, the spread in apparent bulk density is quite large; at a photometric mass of ≈ 100 g, the spread corresponds to a factor of ≈ 10 in bulk density. The Taurids do not show a large spread. Since the Geminid and Taurid meteors are from the same photographic surveys, reduced the same way, and have similar impact speeds (36 and 30 km sec^{-1} or Geminids and Taurids, respectively), we conclude that the spread in the Geminid data is real. If the spread is due to random error, it should have been evident in the Taurid data. An explanation for the spread in apparent bulk density is provided by an elongated shape of the Geminids. This corroborates, but on different grounds, the suggestion by Gustafson (1992), that Geminids are flakes, rather than spheres.

Figure 6-2 suggest that there is a trend in bulk density with meteoroid mass. It appears that high mass Taurids have a larger bulk density (≈ 3 g cm^{-1}) than the lower mass (≈ 0.3 g

cm^{-1}) counterparts. To determine if the trend is real, we need to look closer at how photometric masses are computed.

The conversion from luminous intensity (a measured quantity from meteor photographs) to mass is done with the aid of the third (first and second are the deceleration and mass-loss equations, see chapter 3) fundamental equation of meteor theory, the luminosity equation;

$$I = -\tau \frac{v^2}{2} \frac{dm}{dt},$$

where I is the intensity (total flux) of radiation in a solid angle of 4π steradian, and τ is the luminous efficiency, representing the part of the kinetic energy of the ablated meteoroid material which is transformed into radiation. To find the pre-atmospheric photometric mass, m_{ph}, of the meteoroid, this equation is integrated over the luminous trajectory.

It has been suggested that the luminous efficiency depends mostly on the speed and to a lesser degree on the mass of the meteoroid (see Bronshten, 1983, for a comprehensive review). The Taurids all enter the atmosphere at roughly equal speed, which leaves the mass as a possibility for the trend apparent in Figure 6-2. Unfortunately, there is no experimental data corroborating a mass dependence on the luminous efficiency. However, if the trend is due to a mass dependence on luminous efficiency, we note that the luminous efficiency has to be a factor of ≈ 50 lower for the high mass meteoroids, in order to bring the apparent bulk densities of high mass and low mass Taurids to the same value.

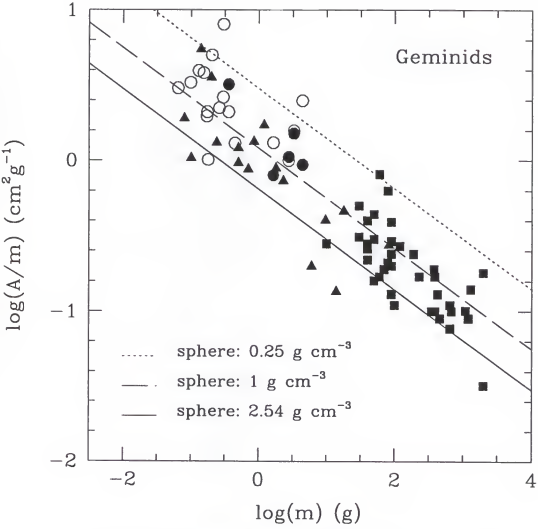

Figure 6-1 Cross-section to mass ratio as a function of photometric mass for Geminids.

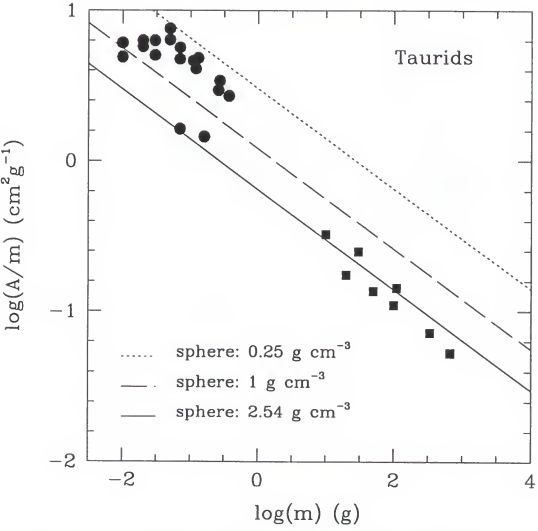

Figure 6-2 Cross-section to mass ratio as a function of photometric mass for Taurids.

CHAPTER 7
RESULTS

Geminids

Integrations performed backward in time of individual recorded Geminid meteors (Kramer & Shestaka, 1986; Gustafson, 1989b) show that Phaethon is a possible parent body to the Geminid meteoroid stream. Further, these investigations show that Phaethon was active within the last 2,000 years, and may even have been within the last 600 years. Therefore, we integrate the equations of motion back to 5,000 BC. Fifty orbits are sampled for each Geminid, and only one orbit is used for Phaethon.

Before we present the results from the Parent-Daughter association method we provide the orbital elements for all Geminids; HSC in Table 7-1, HSS in Table 7-2, and PN in Table 7-3. The angular elements - inclination, i, longitude of ascending node, Ω, and argument of perihelion, ω - refer to the J2000.0 coordinate system (nearly all published meteoroid orbits are given in J1950.0). Published meteoroid orbits lack one orbital element, the true anomaly, f, which is the angle subtended by the Sun-meteoroid and the Sun-perihelion vectors. One cannot start integrations of published orbital elements from the epoch of the meteor, or shortly before, since the meteoroid is still influenced by the Earth's gravitation. Because of this we have chosen to give the true anomaly on January 1, of the year given as second entry in the tables. All orbital elements are provided with one standard deviation errors, originating from the errors in the input data - pre-atmospheric velocity vector and cross-section to mass ratio.

Table 7-1 Orbital elements for HSC Geminids

No.	Yr.	a (AU)	e	i (deg)	Ω (deg)	ω (deg)	f (deg)
1112	1940	1.387 0.001	0.907 0.001	27.2 0.3	259.691 0.004	325.66 0.03	191.7 0.6
1265	1940	1.509 0.004	0.8936 0.0004	21.06 0.04	262.834 < 0.001	320.64 0.04	176.8 0.1
1539	1947	1.294 0.002	0.8946 0.0003	25.30 0.04	262.379 < 0.001	325.49 0.03	169.4 0.1
2283	1950	1.336 0.009	0.898 0.001	22.8 0.1	259.142 < 0.001	325.08 0.03	171.8 0.4
2290	1950	1.277 0.001	0.8910 0.0002	23.00 0.04	260.151 < 0.001	325.08 0.03	168.61 0.07
2293	1950	1.268 0.006	0.898 0.001	19.4 0.1	260.252 < 0.001	325.08 0.04	167.9 0.4
2390	1950	1.268 0.001	0.8883 0.0002	24.22 0.04	262.299 < 0.001	325.08 0.03	167.62 0.09
2377	1950	1.329 0.004	0.8981 0.0003	23.67 0.05	262.447 < 0.001	324.13 0.04	173.3 0.1
2385	1950	1.329 0.004	0.8966 0.0005	23.83 0.08	262.402 < 0.001	325.07 0.02	171.02 0.08
2390	1950	1.353 0.002	0.8952 0.0002	23.39 0.04	262.393 < 0.001	323.70 0.03	172.01 0.09
2390	1950	1.335 0.002	0.8897 0.0002	24.05 0.03	262.379 < 0.001	323.70 0.03	171.02 0.09
2501	1950	1.322 0.009	0.890 0.001	23.3 0.1	261.326 < 0.001	324.21 0.04	170.6 0.5
2537	1950	1.363 0.002	0.8966 0.0002	23.72 0.04	262.385 < 0.001	324.31 0.03	172.49 0.09
2547	1950	1.54 0.20	0.91 0.02	23 2	263.334 0.004	324.2 0.4	176 6
2548	1950	1.328 0.001	0.8922 0.0001	23.40 0.03	261.218 < 0.001	324.31 0.03	170.96 0.04

Table 7-1 -- continued

No.	Yr.	a (AU)	e	i (deg)	Ω (deg)	ω (deg)	f (deg)
2588	1950	1.332 0.004	0.8948 0.0006	22.65 0.07	262.394 < 0.001	324.68 0.03	111.2 0.2
2591	1950	1.39 0.01	0.898 0.001	23.8 0.1	262.349 < 0.001	323.96 0.04	173.4 0.4

Table 7-2 Orbital elements for HSS Geminids

No.	Yr.	a (AU)	e	i (deg)	Ω (deg)	ω (deg)	f (deg)
5605	1950	1.305 0.003	0.8935 0.0004	23.50 0.05	259.838 < 0.001	325.02 0.03	225 4
8645	1950	1.353 0.001	0.8965 0.0002	23.45 0.03	261.781 < 0.001	324.37 0.03	176.7 0.2
9418	1950	1.379 0.001	0.9030 0.0001	21.31 0.04	255.750 < 0.001	325.02 0.03	180.4 0.1
9725	1950	1.351 0.002	0.8942 0.0004	23.79 0.06	262.828 < 0.001	323.98 0.03	176.3 0.4
9749	1950	1.386 0.001	0.8971 0.0001	23.32 0.04	262.877 < 0.001	323.73 0.03	180.7 0.2

Table 7-3 Orbital elements for PN Geminids

No.	Yr.	a (AU)	e	i (deg)	Ω (deg)	ω (deg)	f (deg)
001,003	1965	1.294 0.005	0.8922 0.0005	22.6 0.2	262.297 < 0.001	325.1 0.2	184.9 0.4
013,030	1965	1.271 0.001	0.888 0.001	23.1 0.2	262.659 0.002	324.9 0.2	160 3

Table 7-3 -- continued

No.	Yr.	a (AU)	e	i (deg)	Ω (deg)	ω (deg)	f (deg)
018,020	1965	1.258 0.007	0.881 0.001	21.3 0.2	263.006 0.002	324.1 0.1	154 4
023,024	1965	1.324 0.007	0.8967 0.0007	25.0 0.3	262.908 < 0.001	325.1 0.2	172 1
027,028	1965	1.34 0.02	0.897 0.003	23.8 0.4	262.896 0.002	324.4 0.2	175 4
064,065	1965	1.31 0.01	0.892 0.001	23.8 0.4	262.721 0.002	324.8 0.3	169 1
067,068	1965	1.26 0.01	0.888 0.002	22.4 0.3	262.696 0.003	325.1 0.3	154 4
081,082	1965	1.31 0.02	0.890 0.002	24.3 0.4	262.696 0.005	324.4 0.2	185 3
085,086	1965	1.251 0.008	0.8816 0.0009	21.2 0.3	262.612 0.001	324.3 0.2	174 2
105,106	1965	1.23 0.02	0.892 0.001	22.3 0.6	261.783 0.004	326.4 0.5	161 55
110,111	1965	1.32 0.01	0.894 0.002	24.3 0.4	262.339 0.001	324.8 0.3	187.0 0.9
118,119	1965	1.257 0.006	0.8842 0.0007	21.3 0.2	261.172 < 0.001	324.6 0.2	182.1 0.5
006	1965	1.31 0.01	0.882 0.001	23.1 0.3	262.236 < 0.001	322.3 0.2	188.5 0.9
009	1965	1.31 0.01	0.884 0.001	22.0 0.3	262.409 0.001	323.6 0.2	185.6 0.9
012	1965	1.277 0.008	0.889 0.001	23.0 0.3	262.639 0.002	324.9 0.2	162 2
022	1965	1.370 0.009	0.899 0.001	22.3 0.3	262.947 < 0.001	324.6 0.2	179 1
025	1965	1.236 0.008	0.883 0.001	25.0 0.3	262.313 0.002	325.0 0.2	185 2

Table 7-3 -- continued

No.	Yr.	a (AU)	e	i (deg)	Ω (deg)	ω (deg)	f (deg)
031	1965	1.214 0.008	0.887 0.001	23.6 0.3	262.781 0.002	326.2 0.2	223 70
036	1965	1.256 0.008	0.8905 0.0008	23.4 0.3	261.829 0.002	325.7 0.2	154 4
036	1965	1.46 0.01	0.9120 0.0009	22.0 0.2	260.657 0.003	325.4 0.2	173 1
041	1965	1.299 0.009	0.886 0.001	23.8 0.2	262.762 0.002	323.9 0.3	167 2
044	1965	1.247 0.007	0.8873 0.0009	23.9 0.3	261.827 0.002	325.3 0.2	148 6
060	1965	1.272 0.007	0.8913 0.0009	21.5 0.2	260.856 0.001	325.4 0.2	161 2
060	1965	1.36 0.01	0.900 0.001	24.2 0.2	262.814 < 0.001	324.9 0.2	173 1
060	1965	1.332 0.008	0.8871 0.0009	22.1 0.2	260.732 < 0.001	323.3 0.2	173 1
060	1965	1.349 0.009	0.866 0.001	19.3 0.2	259.773 < 0.001	319.4 0.2	175 1
060	1965	1.36 0.01	0.8982 0.0009	22.3 0.3	262.671 0.001	325.6 0.2	170 2
073	1965	1.38 0.01	0.901 0.001	23.9 0.3	262.692 0.001	324.7 0.2	180 1
076	1965	1.273 0.009	0.8909 0.0009	23.0 0.2	262.802 0.003	325.3 0.2	179 2
079	1965	1.41 0.01	0.885 0.001	20.7 0.2	262.626 0.002	321.0 0.2	190 83
083	1965	1.33 0.01	0.892 0.001	22.9 0.3	262.604 0.003	324.3 0.2	189 2
087	1965	1.26 0.01	0.890 0.001	23.2 0.2	262.500 0.002	325.5 0.2	177 2

Table 7-3 -- continued

No.	Yr.	a (AU)	e	i (deg)	Ω (deg)	ω (deg)	f (deg)
089	1965	1.42 0.01	0.903 0.001	23.8 0.3	262.489 0.004	324.3 0.2	152 66
092	1965	1.254 0.009	0.895 0.001	25.6 0.3	262.409 0.001	326.5 0.2	175 2
093	1965	1.35 0.01	0.900 0.001	23.1 0.2	262.705 0.001	325.1 0.2	195 3
095	1965	1.258 0.007	0.887 0.001	22.1 0.3	261.632 0.001	325.1 0.2	181 1
099	1965	1.31 0.05	0.894 0.008	23.8 0.3	262.612 0.008	325.2 0.3	184 22
102	1965	1.37 0.01	0.895 0.001	23.8 0.3	262.557 0.003	324.6 0.3	201 5
103	1965	1.286 0.009	0.895 0.001	22.5 0.3	262.606 0.003	325.8 0.2	181 1
112	1965	1.293 0.008	0.891 0.001	23.9 0.3	262.379 0.001	324.8 0.2	185 1
115	1965	1.359 0.008	0.8945 0.0009	25.1 0.2	262.277 < 0.001	324.0 0.2	188.9 0.7
124	1965	1.166 0.007	0.879 0.001	26.4 0.3	261.125 < 0.001	326.3 0.3	183 1
127	1965	1.26 0.03	0.895 0.001	25.5 0.6	262.40 0.05	326.4 0.5	176 4

A comparison between the orbital elements in Table 7-1 and those published by Whipple (1954), reveal that the semi-major axis is systematically overestimated by the interpolation polynomial. This is consistent with what Pecina and Ceplecha (1983) found in their investigation. The orbital elements of Table 7-2 are almost identical to those published in Jacchia and Whipple (1961). This is not surprising, since the interpolation polynomial is used

for both estimates. We also note that the HSC and HSS data is nearly an order of magnitude more precise than the PN data. This originate in the fact that the baseline is ten times larger for the PN program than for that of the HSC and HSS programs.

We now turn to the results from the Parent-Daughter association method. None of the sampled Geminid (HSC, HSS, and PN) orbits satisfy the intersection criterion with 1566 Icarus. All Geminids satisfy the intersection criterion with 5786 Talos, but the relative velocity is in excess of 50 km sec^{-1}, far above any reasonable ejection velocity.

Table 7-4 shows seven (of 17) HSC Geminids where the Parent-Daughter association method is applied to Phaethon. All seven Geminids satisfy the intersection condition. Geminids No. 1112, 1265, 1538, and 2290 satisfy neither of the ejection criteria for cometary activity or collision. Geminids No. 2357, 2377 and 2548 satisfy the ejection criterion for cometary activity. The epochs of ejection are over ≈ 5,000 years. This is not consistent with a collisional ejection process.

Table 7-4 HSC Geminids and Phaethon

No.	T_I (years)	$\bar{v}_I$ (km sec^{-1})	$\bar{r}_I$ (AU)	$\bar{\alpha}_I$ (deg)	P (%)
1112	-	-	-	-	-
1265	-	-	-	-	-
1539	-	-	-	-	
2290	-	-	-	-	-
2357	-4250±370	0.51±0.09	0.73±0.12	65±4	17.6
2377	1175±30	0.96±0.04	0.23±0.04	153±3	100.0
2548	-1152±150	1.31±0.04	0.19±0.01	140±4	23.5

Table 7-5 shows the same as Table 7-4, but instead of HSC Geminids, we look at the five HSS Geminids. HSS Geminids 5605 and 9418 do not satisfy the ejection criterion. The potential ejection points from Phaethon for the remaining three HSS Geminids are all close to perihelion, within 0.5 AU, and occurred within roughly the last 1,000 years. Note that two entries are given for 9725 and 9749. This corresponds to the problem we discussed at the end of chapter 4; both nodes may intersect during the same time interval. Only one ejection opportunity is towards the solar hemisphere.

Table 7-5 HSS Geminids and Phaethon

No.	$\bar{T}_I$ (years)	$\bar{v}_I$ (km sec^{-1})	$\bar{r}_I$ (AU)	$\bar{\alpha}_I$ (deg)	P (%)
5605	-	-	-	-	-
8645	810±40	1.2±0.1	0.21±0.03	160±10	80.4
9418	-	-	-	-	-
9725	650±40	0.49±0.03	0.47±0.06	28±12	100.0
9725	650±60	0.79±0.06	0.15±0.03	126±5	100.0
9749	1330±60	0.71±0.06	0.13±0.01	138±8	100.0
9749	1160±30	0.6±0.1	0.17±0.04	112±30	100.0

Table 7-6 shows the outcome when the Parent-Daughter association method is applied to the PN Geminids and Phaethon. Only one PN Geminid (079) did not intersect the orbit of Phaethon. Twenty-two of the 43 PN Geminids have potential ejection points. Eight of twelve PN Geminids with two single-body solutions (indicated by two numbers in the first column) have potential ejection points. The uncertainty in the epoch of ejection, $\sigma(\bar{T}_I)$, increases with how far back the integrations are made. This is reasonable, since the effect of the errors

increases with time in the equations of motion. Roughly 75% of the potential ejection points have $\bar{\alpha}_I \leq 90°$. Further discussion of the results are made in chapter 8.

Table 7-6 PN Geminids and Phaethon

No.	T_I (years)	$\bar{v}_I$ (km sec^{-1})	$\bar{r}_I$ (AU)	$\bar{\alpha}_I$ (deg)	P (%)
001,003	-2540±1030	1.0±0.3	0.2±0.1	108±20	39.2
001,003	-3120±720	0.5±0.2	1.0±0.2	60±20	37.3
013,030	990±400	0.6±0.1	0.9±0.2	90±18	11.8
013,030	-3590±900	0.3±0.1	0.5±0.3	48±30	19.6
018,020	-1630±130	0.42±0.03	1.64±0.05	124±4	15.7
023,024	-	-	-	-	-
027,028	220±520	0.5±0.1	1.1±0.2	78±20	5.9
064,065	-1482±1200	0.4±0.1	0.5±0.3	45±25	96.1
067,068	1140±400	0.3±0.1	1.4±0.3	67±18	29.4
081,082	-	-	-	-	-
085,086	-	-	-	-	-
105,106	1781	0.5	1.3	61	2.0
110,111	-445±630	0.6±0.2	0.8±0.3	57±40	43.1
110,111	-2560±500	0.5±0.3	0.8±0.3	75±30	11.8
110,111	-	-	-	-	-
006	-	-	-	-	-
009	-	-	-	-	-
012	1550±300	0.4±0.1	1.2±0.3	79±10	29.4
012	-3860±900	0.4±0.2	0.7±0.4	87±40	15.7
022	1440±80	1.2±0.2	0.16±0.01	114±9	5.9
022	1240±80	0.73±0.07	0.49±0.08	32±13	47.1
025	-	-	-	-	-

Table 7-6 -- continued

No.	T_I (years)	$\bar{v}_I$ (km sec^{-1})	$\bar{r}_I$ (AU)	$\bar{\alpha}_I$ (deg)	P (%)
031	-	-	-	-	-
036	1800±50	0.5±0.1	1.1±0.2	78±20	5.9
039	-	-	-	-	-
041	-2000±100	0.5±0.1	0.4±0.3	80±16	3.9
044	-	-	-	-	-
050	-	-	-	-	-
051	-	-	-	-	-
059	-	-	-	-	-
069	-	-	-	-	-
069	0±660	0.58±0.04	0.89±0.05	36±6	3.9
073	-	-	-	-	-
076	1740±120	0.5±0.1	1.1±0.2	100±9	11.8
076	-4200±750	0.4±0.1	0.9±0.3	58±28	13.7
076	-	-	-	-	-
083	-60±450	0.4±0.1	0.5±0.2	42±28	37.3
087	1850±70	0.5±0.1	1.1±0.2	90±10	15.7
089	1370±80	0.8±0.1	0.2±0.1	93±26	7.8
092	-	-	-	-	-
093	-	-	-	-	-
095	-	-	-	-	-
099	1590±320	0.5±0.1	1.0±0.3	104±27	11.8
099	-1900±1300	0.5±0.1	0.8±0.2	48±22	25.5
102	1160±90	0.86±0.04	0.4±0.1	157±2	15.7
103	-2210±1160	0.52±0.03	1.0±0.1	40±3	5.9
112	-2550±1200	0.4±0.1	0.9±0.3	45±32	90.2

Table 7-6 -- continued

No.	T_I (years)	$\bar{v}_I$ (km sec^{-1})	$\bar{r}_I$ (AU)	$\bar{\alpha}_I$ (deg)	P (%)
115	-	-	-	-	-
124	-	-	-	-	-
127	900±200	0.9±0.1	0.3±0.1	150±9	39.2

Taurids

Whipple and Hamid (1952) found the Taurids under consideration to have been formed within the last 5,000 years. The dynamics of the Taurid stream is different than the dynamics of the Geminid stream. The Geminids have an aphelion distance of about 2.5 AU, and an inclination of roughly 22 degrees. The Taurids have an aphelion distance of approximately 3-3.5 AU, and an inclination of only a few degrees. The Taurids therefore have a more rapid dynamical evolution, due to its relative closeness to Jupiter. Further, the Taurids are thought to be older than the Geminids, the Taurid stream is more dispersed than the Geminids. We can observe Taurids over a time span of several months, while the Geminids are only present within a few days, with a sharp maximum on December 14. Although these facts discourage us from carrying the integrations too far back in time, we still chose to integrate the Taurids back to AD 20,000. Fifty orbits are sampled for each Taurid. Only the central orbit, neglecting non-gravitational forces, is integrated back in time for P/Encke.

Tables 7-7 and 7-8 show the orbital elements for the HSS and the PN Taurids, respectively. The column entries have the same meaning as in Table 7-1.

Table 7-7 Orbital elements for HSS Taurids

No.	Yr.	a (AU)	e	i (deg)	Ω (deg)	ω (deg)	f (deg)
2961	1950	2.66 0.02	0.870 0.001	2.53 0.02	197.4 0.7	283.4 0.7	183.7 0.2
3886	1950	1.638 0.005	0.807 0.001	1.91 0.02	159.537 < 0.001	123.41 0.04	178.7 0.4
4507	1950	1.518 0.003	0.7927 0.0007	6.36 0.03	358.005 < 0.001	123.41 0.04	178.7 0.4
4701	1950	1.671 0.002	0.8215 0.002	6.36 0.03	7.8622 0.0008	123.76 0.04	191.3 0.2
5022	1950	2.031 0.003	0.8306 0.0003	5.84 0.01	28.678 0.004	115.58 0.04	189.5 0.4
5195	1950	2.01 0.01	0.837 0.001	5.52 0.02	30.72 0.02	117.47 0.04	267 17
5195	1950	2.028 0.002	0.8137 0.0002	5.04 0.01	30.704 0.002	111.90 0.05	310 1
5257	1950	2.130 0.003	0.8774 0.0002	3.13 0.03	214.17 0.05	301.65 0.07	140.5 0.7
5346	1950	2.001 0.006	0.7992 0.0007	5.78 0.02	49.76 0.02	108.62 0.04	246 3
5511	1950	3.38 0.01	0.8979 0.0004	3.20 0.07	7.6 0.3	160.1 0.4	180.6 0.1
8945	1950	1.529 0.002	0.8259 0.0002	5.81 0.03	16.240 0.002	128.23 0.03	239 2
8990	1950	1.109 0.001	0.7570 0.0009	4.15 0.02	16.444 < 0.001	133.97 0.04	193.1 0.6
9015	1950	1.739 0.007	0.8289 0.0009	6.95 0.03	17.70 0.01	122.72 0.05	167.3 0.8
9104	1950	1.726 0.002	0.8237 0.0001	6.10 0.02	27.833 0.002	122.00 0.04	164.5 0.3
9238	1950	1.946 0.005	0.7909 0.0008	5.94 0.02	45.38 0.01	109.49 0.04	182.4 0.4

Table 7-7 -- continued

No.	Yr.	a (AU)	e	i (deg)	Ω (deg)	ω (deg)	f (deg)
9257	1950	2.235 0.004	0.8435 0.0004	2.44 0.02	225.81 0.01	293.68 0.04	202.3 0.4
9331	1950	2.075 0.002	0.8397 0.0001	3.12 0.02	231.623 0.002	196.42 0.03	190.3 0.2
9416	1950	2.172 0.003	0.7583 0.0003	6.48 0.01	75.669 0.002	94.23 0.04	200.0 0.2

Table 7-8 Orbital elements for PN Taurids

No.	Yr.	a (AU)	e	i (deg)	Ω (deg)	ω (deg)	f (deg)
39085	1965	2.48 0.01	0.8233 0.006	2.47 0.05	239.513 0.003	283.2 0.2	196.8 0.1
39093	1965	2.48 0.01	0.8315 0.0007	5.32 0.07	67.425 < 0.001	106.3 0.1	195.4 0.1
39418	1965	2.91 0.02	0.8402 0.0008	16.74 0.05	26.836 < 0.001	99.7 0.1	186.7 0.2
39423	1965	2.12 0.02	0.8848 0.0007	10.3 0.1	211.844 < 0.001	307.4 0.2	174.0 0.4
39424	1965	2.878 0.007	0.8172 0.0004	6.30 0.02	33.040 < 0.001	92.75 0.04	186.64 0.09
39460	1965	2.24 0.01	0.8320 0.0006	6.32 0.06	68.830 < 0.001	111.4 0.1	173.5 0.3
39775	1965	1.948 0.004	0.7566 0.0003	2.32 0.02	198.809 < 0.001	282.52 0.07	243 2
39833	1965	2.316 0.007	0.8311 0.0003	3.47 0.04	256.832 < 0.001	289.11 0.07	149.2 0.7

When comparing the orbital elements of HSS Taurids (Table 7-7), to those of Jacchia and Whipple (1961), we find that the orbital elements are, again, almost identical.

All Taurids satisfy the intersection condition with P/Encke, but none satisfy the ejection condition. Intersections occur over the total integrated time span, almost 22,000 years. The relative velocity is ranging from four to twenty times the gas velocity. We then conclude that we could not genetically relate the Taurids to their proposed parent body, comet P/Encke. A discussion on why we could not link the Taurids to P/Encke is to be found in chapter 8.

CHAPTER 8
DISCUSSION

In the preceding chapter (tables 7-4, 7-5, and 7-6) we find evidence that Geminids (28 out of 55) have probable ejection conditions which favor cometary activity as the ejection process. Probable ejection epochs are distributed over the last 5,000 years, but most of the ejection opportunities are within the last 1,000 years. Further, the ejections occur over a large part of the heliocentric orbit; from ≈ 0.14 AU (perihelion) out to ≈ 1.5 AU. A collision would be expected to yield a narrow bunching in time and location in the orbit.

Figure 8-1 shows the probability of a genetic relation between HSC respectively HSS Geminids with Phaethon, as a function of ejection epoch. Figure 8-2 shows the same as in figure 8-1, but for the PN Geminids. We notice that range in epochs of probable ejections for the massive PN Geminids, is much wider (≈ 5,000 years) than for the less massive HSC and HSS Geminids (≈ 2,000 years).

Figure 8-3 shows the ejection epochs as a function of photometric mass. The filled circles denote HSC and HSS Geminids, and the open circles denote PN Geminids. The solid line indicates the mean catastrophic collisional life time, estimated from Figure 3-1. Note that no ejection epochs are in the part below the solid line. This may be the explanation as to why the HSC and HSS Geminids appear to be younger; small meteoroids are removed from the stream due to catastrophic collisions on a shorter time scale than large meteoroids. However, it should be pointed out that small number statistics plague the HSC and HSS results.

Figure 8-4 shows the ejection points and the direction of ejection for the HSC and HSS Geminids, projected onto the orbit of Phaethon. The dashed circle corresponds to the distance of 1 AU. We see that the ejection points are all close to perihelion, and that the direction of ejection is mostly away from the solar hemisphere. The meteoroids leave Phaethon in a direction such that the specific energy of the heliocentric orbit increases, the Geminid is less bound to the solar system, and the semi-major axis of the meteoroid becomes larger than that for Phaethon. This is also consistent with the orbital elements presented in Tables 7-1 and 7-2. As the meteoroid leaves Phaethon, it immediately feels radiation pressure (effectively reducing the mass of the Sun) which also increases the semi-major axis. However, radiation pressure is not the reason for the large values of the HSC and HSS Geminid semi-major axis with respect to Phaethon. For ejection velocities of a few hundred meters per second, radiation pressure is the dominant process for increasing the semi-major axis when the size of the meteoroid is $\approx$ 30 μm or smaller.

Figure 8-5 shows the same as Figure 8-4, but for the PN Geminids. We notice that the ejection points are more spread around the orbit, but predominantly closer to perihelion than aphelion. The direction of ejection is mostly ($\approx$ 75%) towards the solar hemisphere.

The Parent-Daughter association method is successful in estimating the probability of and the conditions for the ejection of Geminid meteoroids from Phaethon. We confirm Gustafson's (1989b) conclusions that: the Geminids are dynamically related to Phaethon, and that the direction of ejection is skewed towards the solar hemisphere. We also see that the opportunities for ejection span over some 5,000 years, up to quite recently ($\approx$ AD 1,800). These points strongly suggest cometary activity as the source of the Geminids, and that Phaethon once was active, although it now appears to be in a dormant state. Further, now that

we have a rough idea of the ejection conditions, i.e., epoch, ejection velocity (magnitude and direction), and heliocentric distance, it becomes meaningful to carry out forward integrations.

We now investigate what happens if we change the input data to the Parent-Daughter association method. One Geminid from each program (2377 from HSC, 9725 from HSS, and 064,065 from PN) was randomly chosen. Figures 8-6 and 8-7 illustrate what happens when the cross-section to mass ratio is put to zero (open circles), compared to the complete treatment with the cross-section to mass ratio from Tables 5-4, 5-6, and 5-10 (solid circles). Triangles correspond to the results when the Parent-Daughter association method is applied to published orbital elements (Whipple, 1954, and Jacchia & Whipple, 1961). The error bars on the filled circles correspond to the full width of values found at intersection between the sampled meteoroid trajectories and Phaethon.

In Figure 8-6 we plot the ejection velocity, v_{ej} (km sec^{-1}), as a function of heliocentric distance. The dashed line corresponds to the terminal gas speed for cometary activity. All cases yield an ejection velocity below the gas speed. Note that the ejection velocity is lower when the single-body theory is used as opposed to the interpolation polynomial (2377 from HSC). For Geminid 9725 (HSS) we see no clear difference between a finite (filled circle) or a zero value (open circle) of the cross-section to mass ratio. This is probably since the input data is based on the interpolation polynomial in both cases. In Figure 8-7 we plot the ejection angle with respect to the meteoroid-Sun line, α, as a function of ejection epoch. All symbols have the same meaning as in Figure 8-7.

We now compare the D- (Southworth & Hawkins, 1963) and the D'-criterion (Drummond, 1981) to the Parent-Daughter association method. Figure 8-8 shows D versus D' pairings for the Geminids with respect to Phaethon. The dashed line (D' = 0.105) indicates the adopted limit for acceptance according to the D'-criterion. The acceptance limit for the D-

criterion is 0.250, and the line is consequently not shown on the scale. The circles represent those Geminids which are successfully related to Phaethon in terms of the Parent-Daughter association method, and the crosses represent those Geminids that could not be related to Phaethon. We notice that all circles are within the acceptance limits.

Figures 8-9, 8-10, and 8-11 shows the value of the D-criterion as a function of epoch for the three Geminids previously investigated (HSC 2377, HSS 9725, and PN 064,065). The arrows indicate the epoch at which ejection took place. Note that the ejection epoch is not coinciding with the minimum value of the D-criterion. A small value of the D-criterion does not imply that the trajectories of the Parent and the meteoroid intersect. Also note that the value of the D-criterion is smaller than the acceptance limit for stream membership at all epochs for all three Geminids.

How many of the Geminids (55) are sporadic? To answer this question we use the radar meteor data from the IAU meteor data center in Lund, Sweden. The Harvard Radar Synoptic Year consists of 19,818 meteoroid orbits. From the Synoptic Year we remove all Geminids (90), by applying the D'-criterion with an acceptance limit of 0.125. To determine the sporadic background in an orbit similar to the Geminids we search the Synoptic Year by changing the longitude of the ascending node. We then find that there are roughly 4 orbits satisfying the D'-criterion, independent of how we change the longitude of the ascending node. Based on this we estimate that two Geminids are sporadic.

How can we explain the remaining Geminids? First, they may be grand-daughters of Phaethon, Second, non-gravitational forces, mainly A_2, acting on Phaethon may be important (Gustafson, 1992). Third, there may be important forces acting on the meteoroid, which are not taken into account. The Yarkovsky effect, given a suitable spin rate, may be almost as important as radiation pressure on meteoroids close to the Sun (Gustafson, 1994). If a cm-sized

meteoroid contains volatiles after ejection, close to perihelion, the sublimation into free space only takes seconds (Gustafson, 1994). This corresponds to an impulse acting on the meteoroid, and add to the meteoroids ejection velocity

None of the Taurids could be related to P/Encke. This may be due to the fact that the observed non-gravitational forces acting on P/Encke, were not accounted for. This, however, could be accomplished by adopting the non-gravitational terms in the comet's equations of motion (see chapter 4). One problem is that we do not know when to "turn off" the non-gravitational forces. To solve this we would have to sample the values of the non-gravitational terms, as well as the epoch of "turn off." Another explanation may be that P/Encke is not the parent body of the Taurids. It may, for example, be a grand-parent.

Future work is mainly concerned with finding more meteor data. These data have to be of high quality, to allow successful use of Ceplecha's single-body or gross-fragmentation FORTRAN code. It is also desirable to find meteor data for more meteoroid streams. Since the main limitation of the Parent-Daughter association method is computing time, it is also of importance to find analytical expressions for the equations of motion.

Currently, all Harvard photographic plates are stored at the Smithsonian Astrophysical Observatory. The best way to save these plates from deterioration, is to scan them, and save the images in an electronic version. This also has the advantage that better reduction methods (e.g., Ceplecha's single-body code) can be used. Once better reductions are made, we can investigate other phenomena of atmospheric entry, e.g., the rotation of meteoroids (Adolfsson, & Gustafson, 1994; Adolfsson, 1996), and possibly gain insight on the role of the Yarkovsky effect.

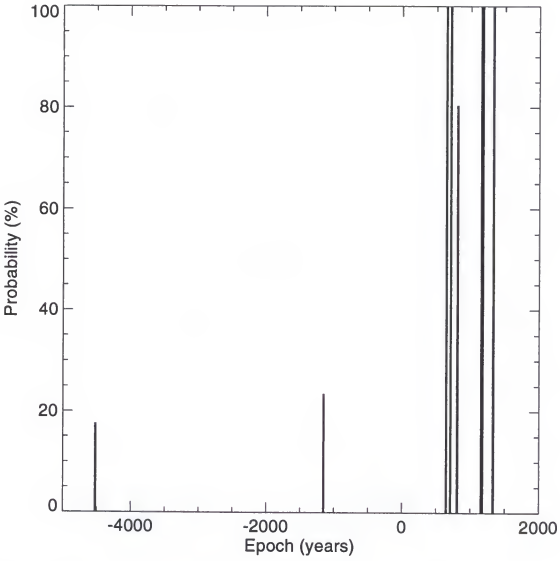

Figure 8-1 Probability of ejection for HSC and HSS Geminids from Phaethon as afunction of epoch.

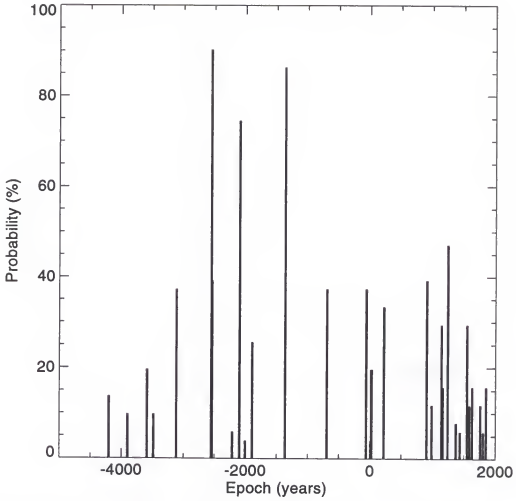

Figure 8-2 Probability of ejection for PN Geminids from Phaethon as a function of epoch.

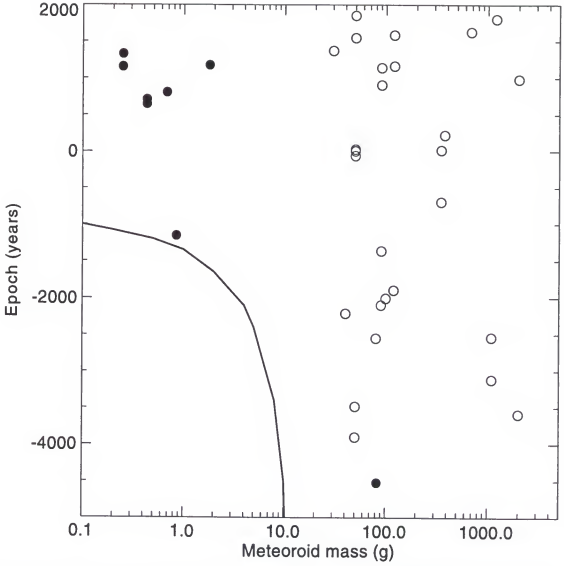

Figure 8-3 Ejection epoch as a function of photometric mass for all Geminids satisfying the criteria for a genetic relation with Phaethon.

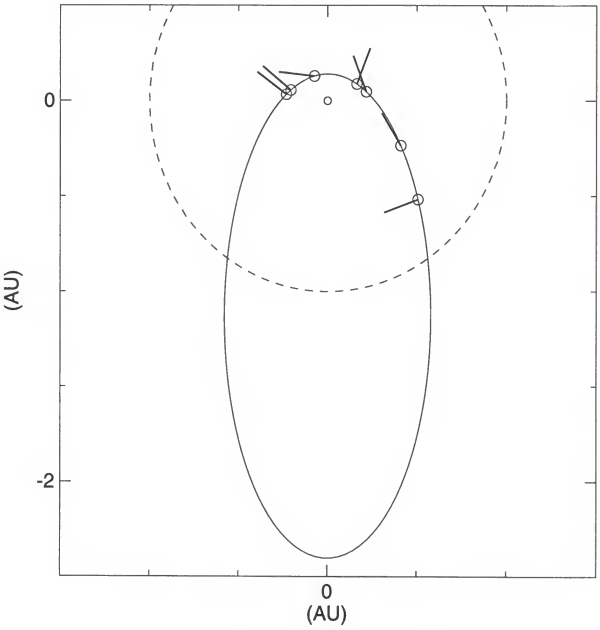

Figure 8-4 Orbital position and direction of the ejection velocity vector for HSC and HSS Geminids.

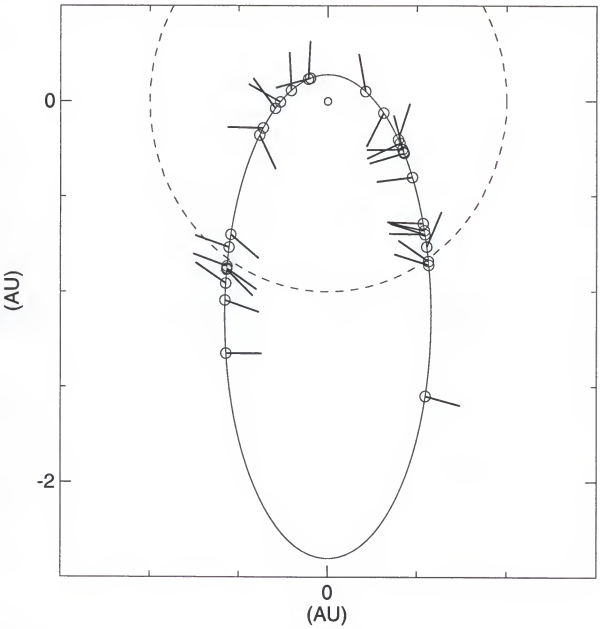

Figure 8-5 Orbital position and direction of the ejection velocity vector for PN Geminids.

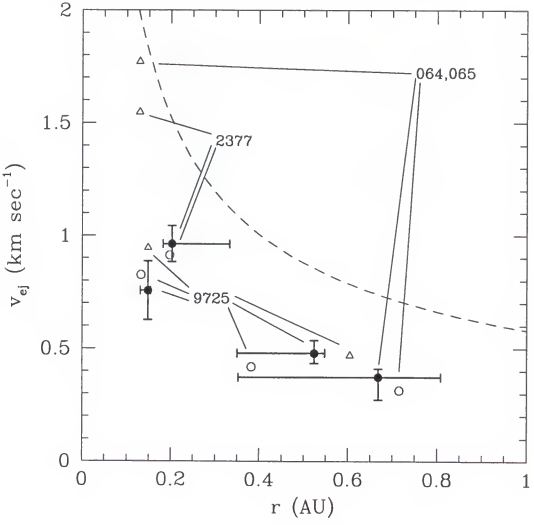

Figure 8-6 Ejection velocity as a function of heliocentric distance for three Geminids.

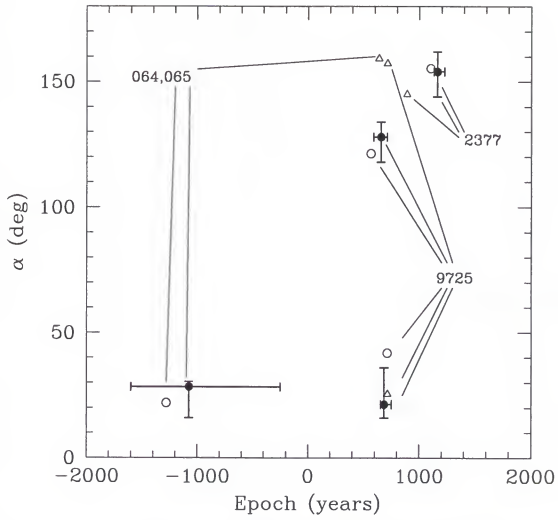

Figure 8-7 Ejection angle wrt the Sun as a function of epoch for three Geminids.

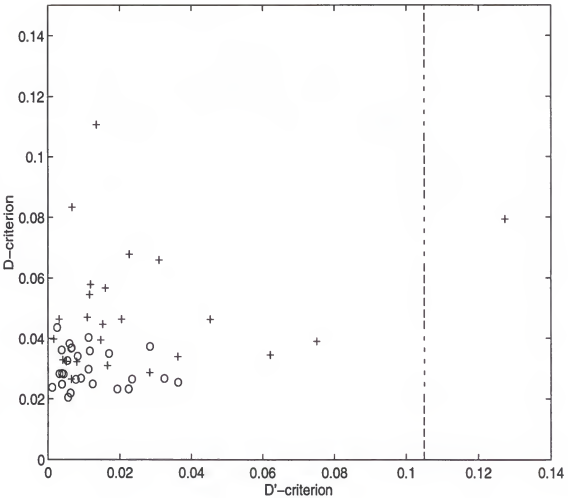

Figure 8-8 D- and D'-criterion for all Geminids.

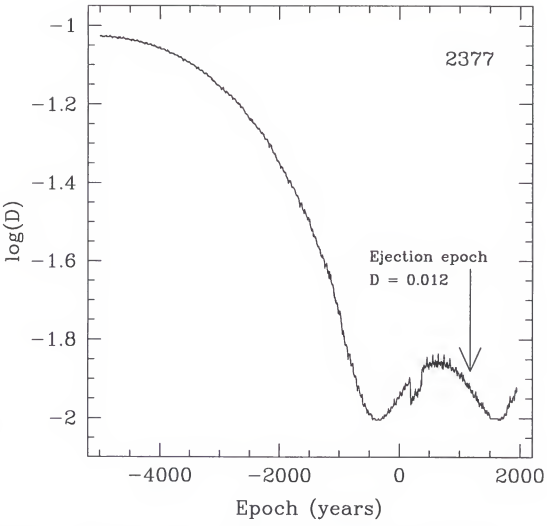

Figure 8-9 D-criterion as a function of epoch for HSC Geminid No. 2377.

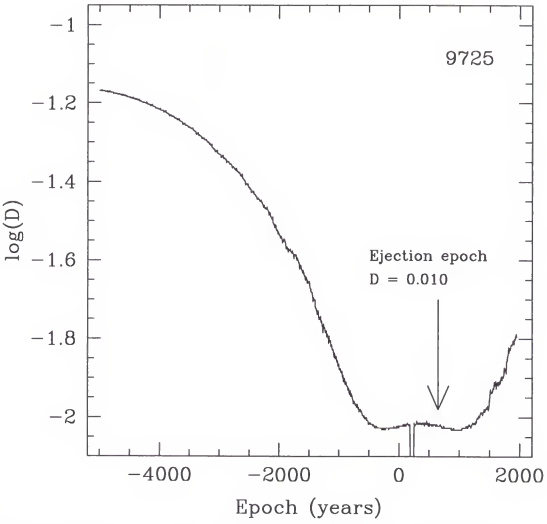

Figure 8-]0 D-criterion as a function of epoch for HSS Geminid No. 9725.

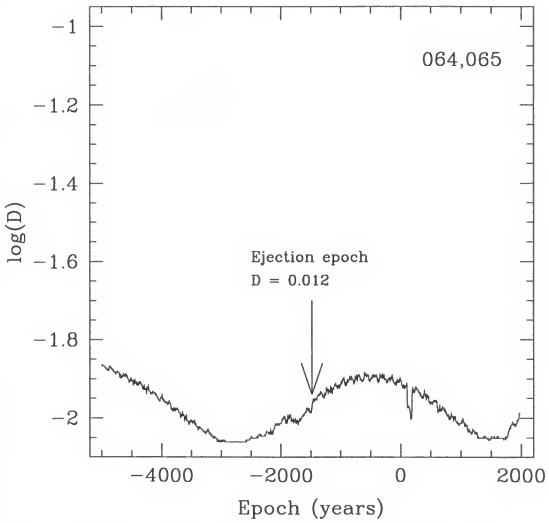

Figure 8-11 D-criterion as a function of epoch for PN Geminid No. 064,065.

CHAPTER 9
CONCLUSION

This is the first time that single-body solutions have been successfully applied to Harvard Small Camera meteors. The new orbital elements show that the non-physical interpolation polynomial overestimates the semi-major axis of the meteoroids heliocentric orbit.

We have developed a rigorous way of determining the meteoroids orbital elements, with uncertainty estimates, from the luminous track (interpreted through single-body theory), through the atmospheric dark flight, into interplanetary space.

Pre-atmospheric cross-section to mass ratios from single-body theory indicate that the Geminids are elongated in shape, and that the apparent bulk density of the Taurids increase with mass.

None out of twenty-four Taurids could be linked to their proposed parent body comet P/Encke.

Twenty-eight of fifty-five Geminids are genetically linked, through the Parent-Daughter association method, to asteroid 3200 Phaethon.

Only about two of the fifty-five Geminids can be attributed to the sporadic background.

The Harvard Small Camera and the Harvard Super-Schmidt Geminids are roughly 1,000 years old. The more massive Prairie Network Geminids have ejection epochs ranging from 5,000 years ago, up to as recent as year 1,800. The apparent difference in age with mass may be due to catastrophic collisions.

The heliocentric distance at ejection range from 0.14 AU to 1.5 AU. The direction of ejection, with respect to the meteoroid-Sun line, is towards the solar hemisphere in roughly 75% of all cases.

The ejections are not close in time and space. This indicates that the Geminids were not formed in a collision event, but rather through cometary activity.

Phaethon was active more or less continuously over the last 5,000 years, up to as recent as year 1,800.

REFERENCES

Adolfsson, L.G., Icarus, submitted (1996).

Adolfsson, L.G., & Gustafson, B.Å.S., Planet. Space Sci. 42, 593 (1994).

Baggaley, W.J., & Taylor, A., Asteroids, Comets, Meteors 1991, Ed. A.W. Harris and E. Bowell, Lunar and Planetary Institute, Houston, p. 33 (1992).

Biermann, L., Z. Astrophys. 29, 274 (1951).

Bronshten, V.A., Physics of Meteoric Phenomena, Reidel, Dordrecht (1983).

Brouwer, D., & Clemence, G.M., Methods of Celestial Mechanics, Academic Press, New York (1961).

Brown, P., & Jones, J., Meteoroids and their Parent Bodies. Ed. I. Štohl and I.P. Williams, Astron. Inst., Slovak Acad. Sci., Bratislava, p. 57 (1993).

Brownlee, D.E., Cosmic Dust, Ed. J.A.M. McDonnell, Wiley-Interscience, New York, p. 295 (1978).

Burns, J.A., Lamy, P.L., & Soter, S., Icarus, 40, 1 (1979).

Carusi, A., Kresák, L., Perozzi, E., & Valsecchi, G.B., Dynamics of Comets: Their Origin and Evolution, Ed. A. Carusi and G.B. Valsecchi, Reidel, Dordrecht, p. 203 (1985).

Ceplecha, Z., Bull. Astron. Inst. Czechosl. 39, 221 (1988).

Ceplecha, Z., Spurný, P., Borovička, J., & Keclíková, J., Astron. Astrophys. 279, 615 (1993).

Cochran, A.L., & Barker, E.S., Icarus. 59, 296 (1984).

Cremonese, G., & Fulle, M., Icarus. 80, 267 (1989).

Crifo, J.F., Intl Proc. Symp. on Radars and Lidars in Earth and Planetary Sci. ESA SP-328, p. 65 (1991).

Crifo, J.F., Itkin, A.L., & Rodinov, A.V., Icarus. 116, 77 (1995).

Delsemme, A.H., Comets, Ed. L.L. Wilkening, University of Arizona Press, Tucson, p. 85 (1982).

Dermott, S.F., Nicholson, P.D., Burns, J.A., & Houchi, J.R., Nature. 312, 505 (1984).

Dermott, S.F., Durda, D.D., Gustafson, B.Å.S., Jayaraman, S., Liou, J.C., & Xu, Y.-L., Asteroids, Comets, Meteors, 1993. Ed. A. Milani, M. Di Martino, and A. Cellino, Kluwer, Dordrecht, p. 127 (1994).

Divine, N., J. Geophys. Res. E98, 17029 (1993).

Drummond, J.D., Icarus. 45, 545 (1981).

Duncan, M., Quinn, T., & Tremaine, S., Astron. J. 94, 1330 (1987).

Duncan, M., Quinn, T., & Tremaine, S., Astrophys J. 328, L69 (1988).

Everhart, E., Dynamics of Comets: Their Origin and Evolution, Ed. A. Carusi and G.B. Valsecchi, Reidel, Dordrecht, p. 185 (1985).

Farinella, P., Froschlé, C., & Gonczi, R., Asteroids, Comets, Meteors, 1993. Ed. A. Milani, M. Di Martino, and A. Cellino, Kluwer, Dordrecht, p. 205 (1994).

Finson, M.L., & Probstein, R.F., Astrophys. J. 154, 327 (1968a).

Finson, M.L., & Probstein, R.F., Astrophys. J. 154, 353 (1968b).

Fox, K., Wiliams, I.P., & Hughes, D.W., Mon. Not. Roy. Astron. Soc. 205, 1155 (1983).

Froschlé, C., Gongzi, R., & Rickman, H., Meteoroids and their Parent Bodies. Ed. I. Štohl and I.P. Williams, Astron. Inst., Slovak Acad. Sci., Bratislava, p. 169 (1993).

Gault, D.E., Shoemaker, E.S., & Moore, H.J., NASA TN D-1767 (1963).

Gombosi, T.I., & Horányi, M., Geophys. Res. Lett. 13, 299 (1986).

Gombosi, T.I., Nagy, A.F., & Cravens, T.E., Rev. Geophys. 24, 667 (1986).

Green, S.F., Meadows, A.J., & Davies, J.K., Mon. Not. Roy. Astron. Soc. 214, 29 (1985).

Greenberg, J.M., & Gustafson, B.Å.S., Astron. Astrophys. 93, 35 (1981).

Greenberg, J.M., & Hage, J.I., Astrophys. J. 361, 260 (1990).

Greenberg, R., Astron. J. 87, 262 (1981).

Grün, E., Gustafson, B.Å.S., Mann, I., Baguhl, M., Morfill, G.E., Staubach, P., Taylor, A., & Zook, H.A., Astron. Astrophys. 286, 915 (1994).

Grün, E., & Jesseberger, E.K., Physics and Chemistry of Comets. Ed. W.F. Huebner, Springer-Verlag, Berlin, p. 113 (1990).

Grün, E., Zook, H.A., Fechtig, H., & Giese, R.H., Icarus. 62, 244 (1985).

Gustafson, B.Å.S., Astrophys. J. 337, 945 (1989a).

Gustafson, B.Å.S., Astron. Astrophys. 225, 533 (1989b).

Gustafson, B.Å.S., Asteroids, Comets, Meteors, III. Ed. C.-I. Lagerqvist, H. Rickman, B.A. Lindblad, and M. Lindgren, Uppsala Universitet, Reprocentralen HSC, Uppsala, Sweden, p. 523 (1992).

Gustafson, B.Å.S., Ann. Rev. Earth Planet. Sci. 22, 553 (1994).

Gustafson, B.Å.S., & Adolfsson, L.G., Earth, Moon, and Planets. 72, 327 (1996).

Hanner, M.S., Cometary Exploration. Ed. T.I. Gombosi, Central Research Institute for Physics, Hungarian Academy of Sciences, Budapest, II, p. 1 (1983).

Hawkes, R.L., Meteoroids and their Parent Bodies. Ed. I. Štohl and I.P. Williams, Astron. Inst., Slovak Acad. Sci., Bratislava, p. 227 (1993).

Hoppe, J., Astron. Nachr. 262, 169 (1937).

Huebner, W.F., Physics and Chemistry of Comets. Ed. W.F. Huebner, Springer-Verlag, Berlin, p. 1 (1990).

Hughes, D.W., Meteoroids and their Parent Bodies. Ed. I. Štohl and I.P. Williams, Astron. Inst., Slovak Acad. Sci., Bratislava, p. 15 (1993).

Jacchia, L.G., Harvard College Observatory TN-10 (1952).

Jacchia, L.G., Verniani, F., & Briggs, R.E., Smithson. Contr. Astrophys. 10, 1 (1967).

Jacchia, L.G., & Whipple, F.L., Vistas in Astronomy. 4, 97 (1956).

Jacchia, L.G., & Whipple, F.L., Smithson. Contr. Astrophys. 4, 97 (1967).

Jenniskens, P., Astron. Astrophys. 295, 206 (1995).

Keller, H.U., Cometary Exploration. Ed. T.I. Gombosi, Central Research Institute for Physics, Hungarian Academy of Sciences, Budapest, II, p. 119 (1983).

Kirkwood, D., Danville Quart. Rev. 1, 614 (1861).

Klačka, J., Earth, Moon and Planets. 59, 41 (1992).

Kramer, E.N., & Shestaka, I.S., Kinematika i Fizika Nebesnykh Tel. 2, 81 (1986).

Kuiper, G.P., Astrophysics. Ed. J.A. Hynek, McGraw Hill, New York, p. 357 (1951).

Luu, J., Asteroids, Comets, Meteors, 1993. Ed. A. Milani, M. Di Martino, and A. Cellino, Kluwer, Dordrecht, p. 31 (1994).

Luu, J., & Jewitt, D.C., Icarus. 86, 69 (1990).

Malaise, D.J., Astron. Astrophys. 5, 209 (1970).

Marconi, M.L., & Mendis, D.A., Astrophys. J. 287, 445 (1984).

Marsden, B.G., Sekanina, Z., & Yeomans, D.K.,Astron. J. 78, 211 (1979).

Marsden, B.G., & Williams, G.V., Catalogue of cometary orbits, Eighth edition. International Astronomical Union, Central bureau for astronomical telegrams, Minor planet center, Cambridge (1993).

McCrosky, R.E., & Boeschenstein, H. Jr., Smithsonian Astrophysical Observatory, SP-173 (1965).

McCrosky, R.E., & Posen, A., Smithsonian Astrophysical Observatory, SP-273 (1968).

McCrosky, R.E., Posen, A., Schwartz, G., & Shao, C.Y., J. Geophys. Res. 76, 4090 (1971).

Muionen, K. & Bowell, E., Icarus. 104, 255 (1993).

Nakamura, A., & Fujiwara, A., Icarus. 92, 132 (1991).

Oort, J.H., Bull. Astron. Inst. Neth. 11, 91 (1950).

Öpik, E., Proc. Roy. Ir. Acad.. 54, 165 (1951).

Öpik, E., Adv. Astron. Astrophys. 2, 219 (1963).

Pecina, P., Bull. Astron. Inst. Czechosl. 40, 67 (1989).

Pecina, P., Planet. Space Sci. 42, 677 (1994).

Pecina, P., & Ceplcha, Z., Bull. Astron. Inst. Czechosl. 34, 102 (1983).

Pecina, P., & Ceplcha, Z., Bull. Astron. Inst. Czechosl. 35, 120 (1984).

Peterson, C., Icarus. 29, 91 (1976).

Press, W.H., Flannery, B.P., Teukolsky, S.A., & Vetterling, W.T., Numerical Recipes. Cambridge University Press, Cambridge (1992).

Probstein, R.F., Problems of Hydrodynamics and Continuum Mechanics. Ed. M.A. Larent'ev, Soc. Industr. Appl. Math., Philadelphia, p. 78 (1969).

Rickman, H., Adv. Space Res. 9, 59 (1989).

Rickman, H., Fernández, J.A., & Gustafson, B.Å.S., Astron. Astrophys. 237, 524 (1990).

Robertson, H.P., Mon. Not. Roy. Astron. Soc. 97, 423 (1937).

Schiaparelli, G.V., Astron. Nachr. 68, 331 (1867).

Sekanina, Z., Icarus. 13, 459 (1970).

Sekanina, Z., Astron. J. 105, 702 (1993).

Southworth, R.B., & Hawkins, G.S., Smithson. Contr. Astrophys. 7, 261 (1963).

Sykes, M.V., & Walker, R.G., Icarus. 95, 180 (1992).

Valtonen, M.J., & Innanen, K.A., Astrophys. J. 255, 307 (1982).

van de Hulst, H.C., Light Scattering by Small Particles. Wiley, New York (1957).

Weigert, A., Astron. Nachr. 285, 117 (1959).

Whipple, F.L., Proc. Amer. Phil. Soc. 79, 499 (1938).

Whipple, F.L., Proc. Amer. Phil. Soc. 91, 119 (1947).

Whipple, F.L., Proc. Amer. Phil. Soc. 136, 687 (1950a).

Whipple, F.L., Astrophys. J. 111, 375 (1950b).

Whipple, F.L., Astrophys. J. 114, 464 (1951).

Whipple, F.L., Astron. J. 59, 201 (1954).

Whipple, F.L., & Hamid, S.E.D., Helwan Observatory Bulletin. 41, 499 (1952).

Whipple, F.L., & Jacchia, L.G., Smithson. Contr. Astrophys. 1, 183 (1957).

Whipple, F.L., & Sekanina, Z., Astron. J. 84, 1894 (1979).

Yeomans, D.K., Asteroids, Comets, Meteors, 1993. Ed. A. Milani, M. Di Martino, and A. Cellino, Kluwer, Dordrecht, p. 241 (1994).

Zappalà, V., Farinella, P., Knežević, Z., & Paolicchi, P., Icarus. 59, 261 (1984).

Zook, H.A., Grün, E., Baguhl, M., Hamilton, D., Linkert, G., Liou, J.-C, Forsyth, R., & Phillips, J.L., Physics, Chemistry and Dynamics of Interplanetary Dust. Ed. B.Å.S. Gustafson and M.S. Hanner, Astron. Soc. of the Pacific Press, in press (1996).

BIOGRAPHICAL SKETCH

Lars Göran Adolfsson was born on the 10th of March 1967 in Stockholm, Sweden. He is the son of Karin and Hugo Adolfsson. In 1986 he began to study at the Royal Institute of Technology in Stockholm, pursuing a masters degree in Engineering Physics. During 1988-89 he was on "leave" from science, as he did service in the Swedish army. Just to be sure that he had made the right choice when entering the scientific arena, he studied one year at the Stockholm School of Economics. After realizing what the difference between quantity and quality was, he quit economics and went back full time to "real" science. In January 1992 he finally got his masters degree. During the summer of 1991 he completed his masters thesis at the Department of Astronomy, University of Florida, under the supervision of Dr. Bo Gustafson. This collaboration was fruitful, and he soon (summer 1992) found himself enrolled in the graduate program at the University of Florida. Lars will receive his doctorate degree in May of 1996.

In July 1993 Lars and his wife, Madeleine Steiner-Adolfsson, became parents; Christopher Marc Io Adolfsson was born into this world. Almost exactly two years later, a little girl, Danniella Vendela Dione Adolfsson, joined the Adolfsson family.

I certify that I have read this study and that in my opinion it conforms to acceptable standards of scholarly presentation and is fully adequate, in scope and quality, as a dissertation for the degree of Doctor of Philosophy.

Bo Å. S. Gustafson, Chair
Associate Professor of Astronomy

I certify that I have read this study and that in my opinion it conforms to acceptable standards of scholarly presentation and is fully adequate, in scope and quality, as a dissertation for the degree of Doctor of Philosophy.

Stanley F. Dermott
Professor of Astronomy

I certify that I have read this study and that in my opinion it conforms to acceptable standards of scholarly presentation and is fully adequate, in scope and quality, as a dissertation for the degree of Doctor of Philosophy.

Humberto Campins
Associate Professor of Astronomy

I certify that I have read this study and that in my opinion it conforms to acceptable standards of scholarly presentation and is fully adequate, in scope and quality, as a dissertation for the degree of Doctor of Philosophy.

Carl D. Murray
Assistant Professor of Astronomy

I certify that I have read this study and that in my opinion it conforms to acceptable standards of scholarly presentation and is fully adequate, in scope and quality, as a dissertation for the degree of Doctor of Philosophy.

Yngve Öhrn
Professor of Chemistry

This dissertation was submitted to the Graduate Faculty of the Department of Astronomy in the College of Liberal Arts and Sciences and to the Graduate School and was accepted as partial fulfillment of the requirements for the degree of Doctor of Philosophy.

May, 1996

Dean, Graduate School